Alkynes in covalent enzyme inhibitors: down the kinetic rabbit hole
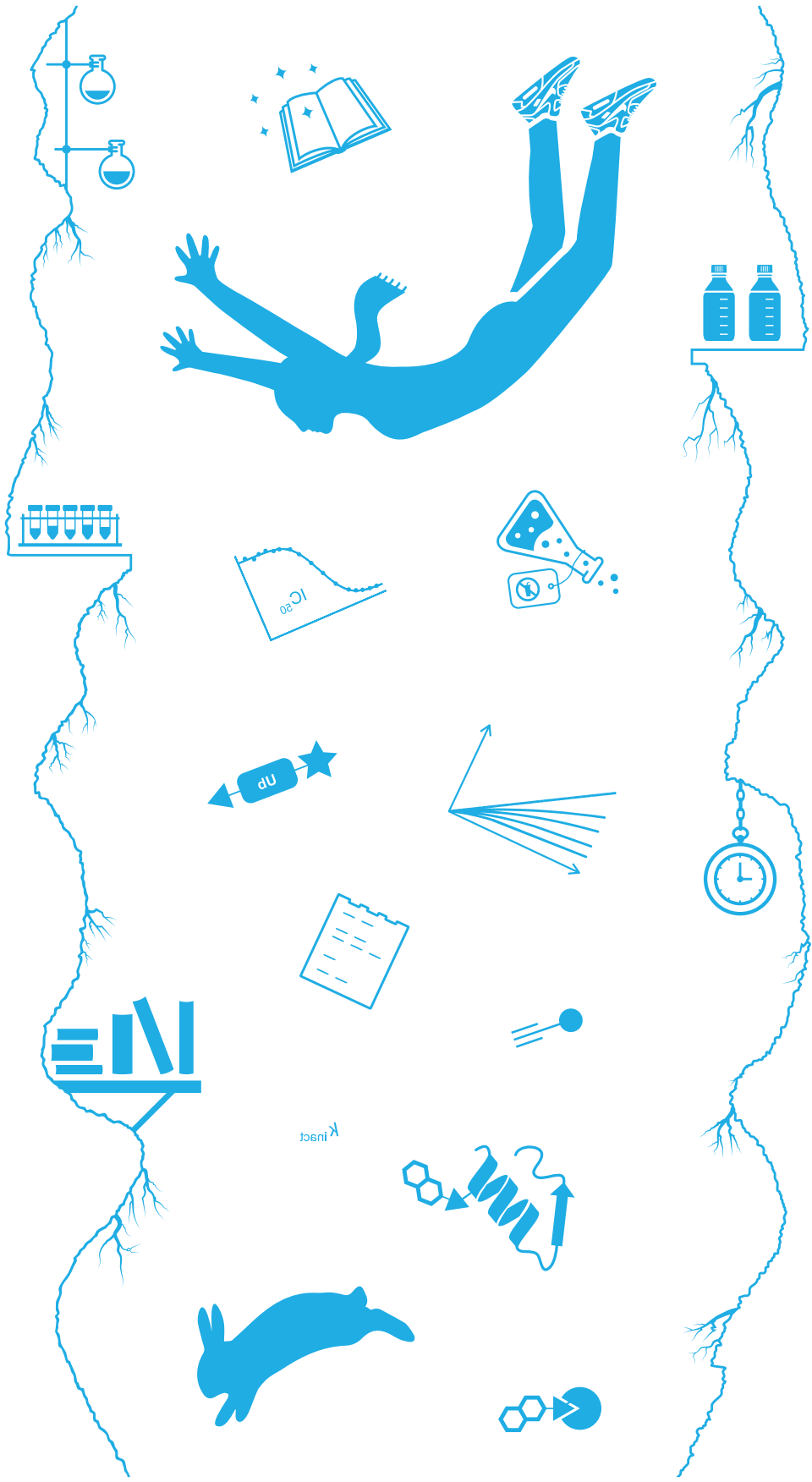
Mons, E.

Chapter 4

Nonactivated Alkynes in Irreversible Covalent Cathepsin K Inhibitors

Abstract. Irreversible covalent inhibitors can have a beneficial pharmacokinetic/ pharmacodynamics profile but are still often avoided due to the risk of indiscriminate covalent reactivity and the resulting adverse effects. To overcome this potential liability, we introduced an alkyne moiety as a latent electrophile into small molecule inhibitors of cathepsin K (CatK). Alkyne-based inhibitors do not show indiscriminate thiol reactivity but potently inhibit CatK protease activity by formation of an irreversible covalent bond with the catalytic cysteine residue, confirmed by crystal structure analysis. The rate of covalent bond formation (k_{inact}) does not correlate with electrophilicity of the alkyne moiety, indicative of a proximity-driven reactivity. Inhibition of CatK-mediated bone resorption is validated in human osteoclasts. Together, this work illustrates the potential of alkynes as latent electrophiles in small molecule inhibitors, enabling the development of irreversible covalent inhibitors with an improved safety profile.
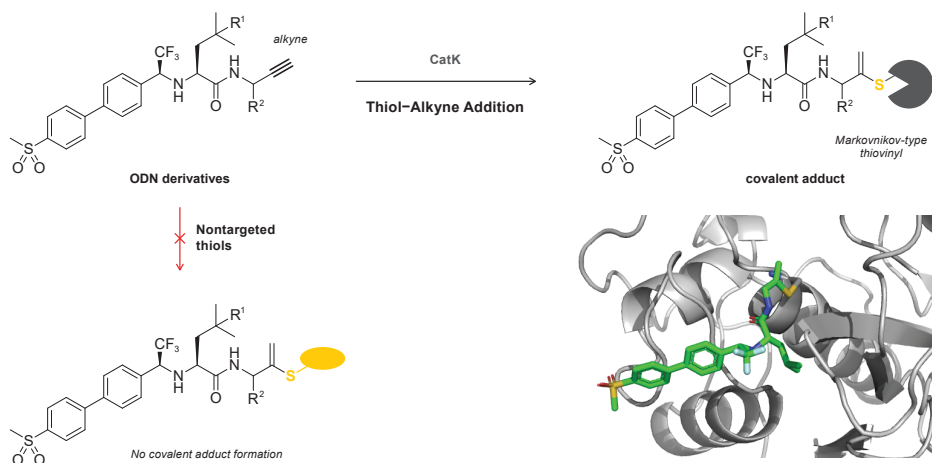
1. Introduction

Irreversible covalent inhibition of a target protein minimizes the required systemic drug exposure as protein activity can only be restored by *de novo* protein synthesis, resulting in a prolonged therapeutic effect long after the compound is cleared from the blood.[1-2] Strategically placing an electrophilic moiety on the inhibitor will allow it to undergo attack by a nucleophilic amino acid residue upon binding to the target protein, forming a(n) (ir)reversible bond that is much stronger than typical noncovalent interactions. However, the ability to form a covalent bond with the target enzyme has raised concerns about indiscriminate reactivity with off-target proteins,[3-5] even though some of the most prescribed drugs are covalent irreversible binders.[6-7] This led to the disfavor of covalent modifiers as drug candidates until the recent successful development of irreversible covalent kinase inhibitors ibrutinib and afatinib, which form an irreversible covalent bond between an acrylamide warhead and a nonconserved cysteine residue on the ATP-binding site[2, 8-10] but also with nontargeted cellular thiols.[11] The ability to form covalent adducts with off-target proteins has been linked to an increased risk of unpredictable idiosyncratic toxicity along with the daily drug dose administered to patients.[11-14] This risk can be reduced by incorporating less reactive electrophilic moieties into irreversible covalent inhibitors.

Terminal alkynes are generally considered "inert" toward cellular components – in absence of radical initiators, metal catalysts, and metabolic activators – and are therefore often used in bioorthogonal approaches as chemoselective "Click" handles.[15-16] However, our group has shown a C-terminal propargyl moiety on ubiquitin to react in an activity-based manner with the catalytic cysteine residue in deubiquitinating enzymes (DUBs), forming an irreversible thioether bond *via* an *in situ* thiol–alkyne addition (**Figure 1A**).[17] Markovnikov hydrothiolation of (terminal) alkynes with aliphatic thiols has been described for metal-catalyzed reactions,[19-22] but has not been reported to occur outside the active site of a cysteine

4

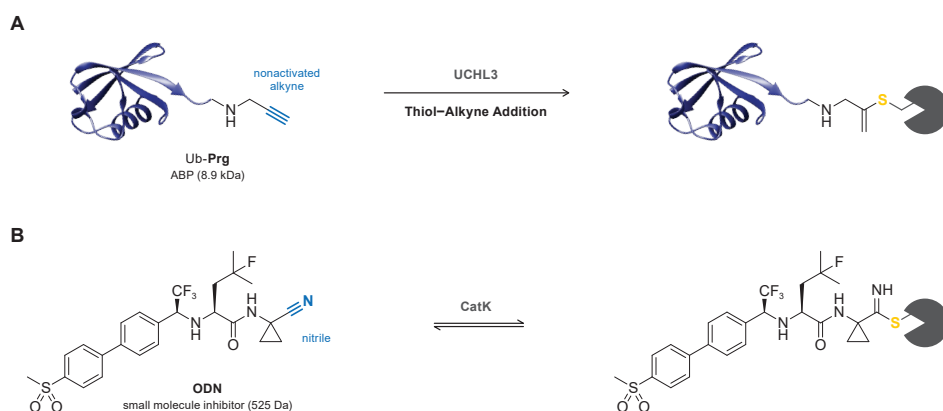**Figure 1 |** Terminal alkyne moiety as latent electrophile for thiol–alkyne addition. **(A)** ABPs with ubiquitin recognition element and propargyl (**Prg**) warhead covalently modify the catalytic Cys in CysDUB proteases, forming a Markovnikov-type thiovinyl adduct. **(B)** The nitrile warhead in the established covalent inhibitor odanacatib (ODN) forms a reversible covalent adduct with catalytic Cys25 of cysteine protease CatK.[18]

protease under physiological conditions. The alkyne moiety on ubiquitin did not react with cysteine residues present in nontargeted proteins nor with excess thiol. Work by Sommer *et al.* revealed that the catalytic triad does not have to be intact for covalent bond formation, indicating a proximity-driven reactivity.[23] It is believed that the reactivity of the alkyne resulted from a template effect – recognition of (large) protein fragments driving the formation of the thermodynamically unfavored Markovnikov-type thiovinyl product[24] – and here we show that strong enough binding can be achieved with a small molecule recognition part. This study highlights the potential of alkynes as latent electrophiles in irreversible covalent small molecule inhibitors, as demonstrated for cathepsin K (CatK). CatK is a cysteine protease that is highly expressed in osteoclasts and is the most important protease in bone degradation.[25] Implicated in diseases such as osteoporosis, its inhibition has been of therapeutic interest for the past decade.[26] The most promising small molecule CatK inhibitor to date was odanacatib (ODN),[18] a nonlysosomotropic inhibitor with a nitrile moiety as reversible covalent warhead that binds to catalytic Cys25 (**Figure 1B**). ODN has a high selectivity for CatK versus other cathepsins and only has to be taken once weekly because of its very long half-life of 66-93 h.[27] Clinical development was terminated after phase III clinical trials showed side effects including increased stroke risks and cardiovascular events.[28-30] It is currently unclear whether this is due to inhibition of nonskeletal degradation properties of CatK or because of off-target inhibition.[31] Nonetheless, the close proximity of the nitrile moiety relative to Cys25 made it a suitable model to incorporate an alkyne moiety as electrophile.

2. Results and Discussion

Synthesis and design. Derivatives of ODN were obtained by functionalization of precursor **1**, according to reported procedures (**Figure 2**, **Scheme S1**).[32-33] Replacing the nitrile with an alkyne led to compromised solubility in aqueous media for alkyne EM03, which could be overcome by removal of the hydrophobic cyclopropane in nitrile EM02, propargyl EM04, and monomethylated propargyl EM05. The cyclopropane moiety is not essential for CatK inhibition but was introduced in the development of ODN to reduce metabolic liabilities.[18] Alkyne electrophilicity increases if an electron-withdrawing substituent is introduced on the terminal position,[20, 34] while remaining less electrophilic than acrylamides. Therefore, electron-
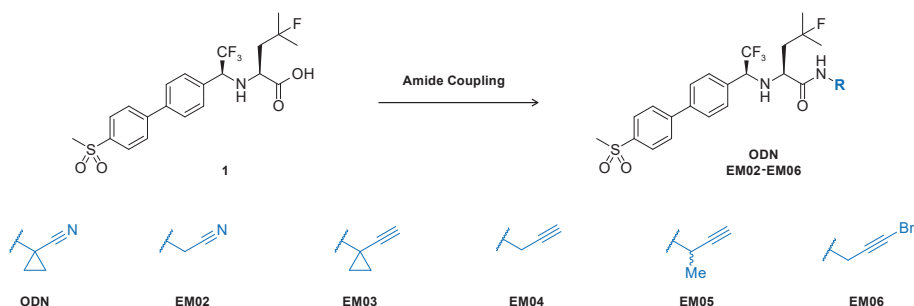

Figure 2 | Design of nitriles **ODN** and **EM02**, nonactivated alkyne analogues **EM03-EM05**, and electron-deficient bromoalkyne analogue **EM06**. Synthesis and yields can be found in **Scheme S1**.

deficient alkyne EM06 was taken along to investigate the effect of electrophilicity on the inhibitor selectivity. Conjugate addition of cysteine has been reported for electron-deficient internal alkynes such as the 2-butynamide warhead – the electrophile in irreversible covalent BTK inhibitor acalabrutinib.[20, 35-36]

Indiscriminate thiol reactivity. Indiscriminate thiol reactivity was assessed following an established protocol in which nitrile-based inhibitors form an irreversible covalent adduct with cysteine (**Figure 3**).[37] Nitrile-based inhibitors ODN and EM02 show adduct formation that increases upon increasing the pH of the buffer, as do acrylamide-based kinase inhibitors ibrutinib and afatinib, and irreversible pan-cathepsin inhibitor E-64.[38] The cysteine adduct was not detected for alkyne-based inhibitors EM03, EM04, and EM05, supporting our hypothesis that the nonactivated alkyne is not reactive toward cysteine residues in nontargeted proteins. As expected,[36] adduct formation with electron-deficient alkynes EM06 and acalabrutinib was observed, underlining the importance of alkyne electrophilicity in indiscriminate thiol reactivity. Glutathione (GSH), a tripeptide with a cellular concentration of 0.5-10 mM,[39] is a commonly used biological thiol to assess the risk of idiosyncratic toxicity. Covalent adduct was observed upon incubation with 5 mM GSH for acrylamides and electron-deficient alkynes, as reported,[11, 36] but not for any of the nitriles or nonactivated alkynes. The lack of nitrile adduct detection with nitriles ODN and EM02 is not representative, as these form a reversible covalent adduct with GSH that quickly dissociates under denaturing conditions.

In vitro **inhibition.** A recurring issue in CatK drug development is the difference in amino acids at the active site for rodentCatK compared to humanCatK, thus reducing the apparent potency of ODN up to 182-fold in mice and rats.[40] The potency of our inhibitors was assessed

4

Compound	Electrophile	Cysteine adduct			GSH
		pH 5.5	pH 7.5	pH 8.0	pH 7.5
ODN	nitrile	<1%	17%	48%	<1% *
EM02	nitrile	5%	91%	98%	<1% *
EM03	alkyne	<1%	<1%	<1%	<1%
EM04	alkyne	<1%	<1%	<1%	<1%
EM05	alkyne	<1%	<1%	<1%	2%
EM06	bromoalkyne	<1%	55%	66%	47%
E-64	epoxysuccinate	<1%	68%	79%	64%
afatinib	acrylamide	92%	98%	95%	94%
ibrutinib	acrylamide	9%	99%	96%	91%
acalabrutinib	2-butynamide	19%	98%	97%	95%
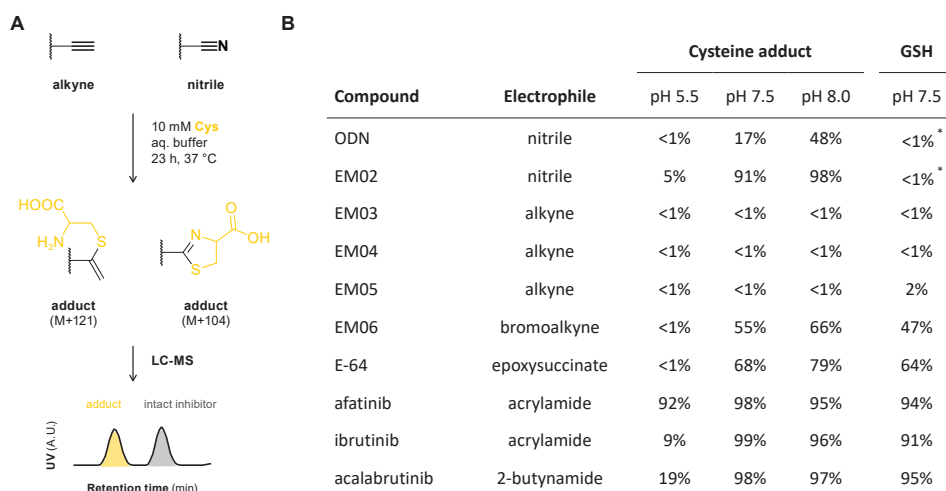
Figure 3 | Indiscriminate thiol reactivity assessed by LC-MS analysis following established protocol.[37] **(A)** Schematic overview. Thiol adducts formed upon incubation with cysteine are quantified from LC-MS UV traces. Nitrile warheads form an irreversible adduct with cysteine. **(B)** Adduct formation upon 23 h incubation with 10 mM cysteine or 5 mM GSH at 37 °C in aqueous buffer. Details in **Table S1**. * Reversible adduct.

in an *in vitro* activity assay on recombinant human cathepsins (**Table 1**). As reported, ODN is selective for hCatK with an IC_{50} below 1 nM. Noncovalent interactions were optimized for ODN, and we anticipated that replacing the polarized nitrile moiety by a nonpolarized alkyne moiety would decrease the noncovalent interaction with active site residues, thereby reducing the noncovalent affinity (K_i). This is indeed reflected in increased IC_{50} values for all alkyne-based inhibitors. Selectivity for CatK over related human cathepsins CatS, CatV, CatL, and CatB was conserved for alkynes EM04 and EM05, while all selectivity is lost for electron-deficient alkyne EM06. Inhibition of hCatK activity was validated in a gel-based probe labeling experiment with quenched activity-based probe (qABP) BMV109 (**Figure S2**).

Binding mode of alkynes is irreversible and covalent. Reversibility of hCatK inhibition was assessed in a jump dilution assay.[41] Recombinant hCatK was incubated with inhibitor at high concentration to allow full active site occupation and subsequently diluted 300-fold into fluorogenic substrate (Z-FR-AMC) solution (**Figure 4**). For reversible inhibitors, rapid/jump dilution induces inhibitor dissociation from the enzyme when the inhibitor concentrations before and after dilution span the IC_{50}, resulting in an increase of substrate hydrolysis. For inhibitors with an irreversible binding mode, dilution does not induce inhibitor dissociation and does not affect enzyme inhibition. The progress curves show that ODN is a (fast) reversible inhibitor, while inhibition by alkynes EM04, EM05, and EM06 is irreversible. The covalent nature of the cathepsin–inhibitor interaction was elucidated by LC-MS analysis of intact CatK and CatK–inhibitor adducts (**Figure 5**). An increase in the deconvoluted mass corresponding to addition of the inhibitor to hCatK was observed for nitrile ODN and alkynes EM04, EM05, and EM06, confirming the formation of a covalent hCatK–inhibitor adduct. For ODN, unbound CatK was predominantly detected despite the inhibitor concentration far above the K_i^*. This

Table 1 | IC_{50} values (nM) against proteolytic activity of recombinant purified cysteine proteases.

	hCatK	hCatL	hCatS	hCatV	hCatB	papain
ODN	0.56 ± 0.0022	$(5.8 \pm 0.72) \times 10^3$	24 ± 0.57	600 ± 40	63 ± 2.5	690 ± 58
EM02	0.57 ± 0.0090	$>10^3$	18 ± 0.30	910 ± 110	21 ± 0.66	230 ± 12
EM03	$(26 \pm 2.2) \times 10^3$	$>10^5$	$>10^5$	$>10^5$	$>10^5$	$>10^5$
EM04	290 ± 8.7	$>10^5$	$(11 \pm 0.84) \times 10^3$	$(24 \pm 1.4) \times 10^3$	$(9.4 \pm 0.63) \times 10^3$	$(14 \pm 1.8) \times 10^3$
EM05	350 ± 12	$>10^5$	$(16 \pm 1.8) \times 10^3$	$(46 \pm 2.3) \times 10^3$	$(40 \pm 4.4) \times 10^3$	$(22 \pm 3.9) \times 10^3$
EM06	47 ± 1.8	100 ± 4.6	55 ± 2.9	16 ± 0.88	99 ± 5.9	$(6.3 \pm 0.73) \times 10^3$
EM07	351 ± 7.6	N.A.	N.A.	N.A.	N.A.	N.A.
E-64	1.9 ± 0.032	3.4 ± 0.18	N.A.	N.A.	N.A.	2.4 ± 0.82

Preincubation of human cysteine protease and inhibitor for 30 min prior to addition of fluorogenic substrate. Mean ± SD for a single representative experiment (triplicate measurement). N.A. = not available. Dose-response curves are available in **Figure S1**.

is probably due to the reversible covalent binding mode; the denaturing conditions of LC-MS analysis induce reversible inhibitor dissociation, but the off-rate for ODN is slow enough to still detect the adduct.
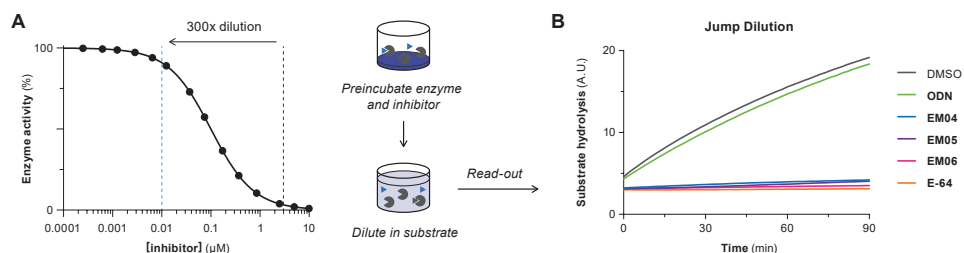

Figure 4 | Jump dilution assay to evaluate reversibility of inhibitor binding. **(A)** Principle of jump dilution. 300-fold dilution results in inhibitor concentrations corresponding to full inhibition *(before dilution)* to full activity *(after dilution)*. **(B)** Progress curves for hCatK proteolytic activity after dilution in 4 µM Z-FR-AMC. *Control:* E-64 is an irreversible pan-cathepsin inhibitor. Progress curves for control samples (without dilution) are available in **Figure S3**.
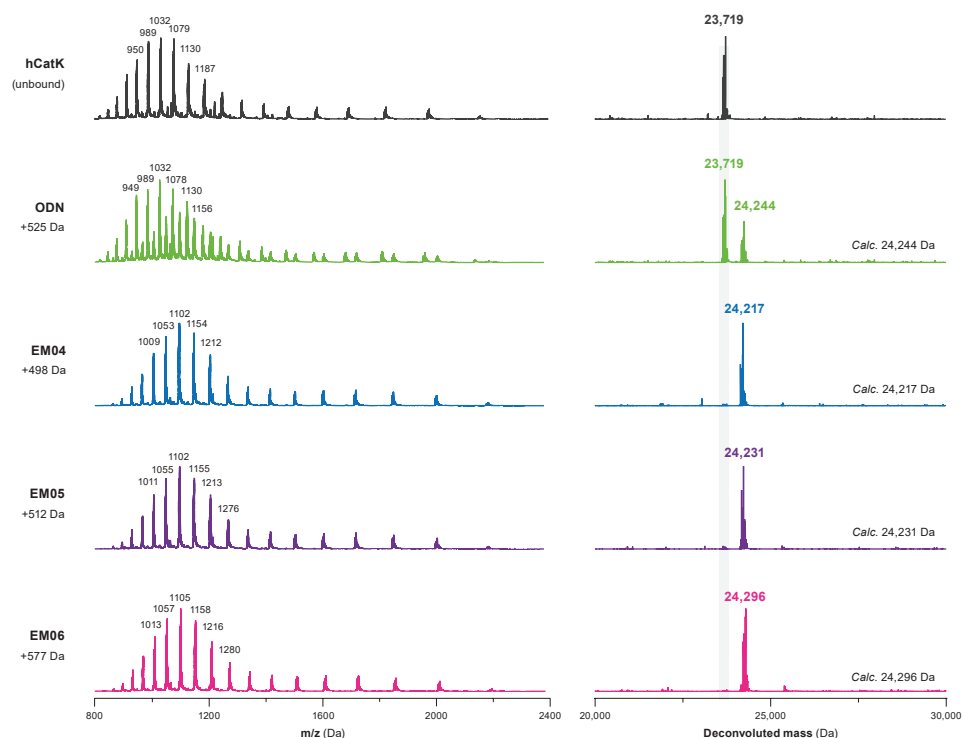

Figure 5 | Intact protein MS analysis. Representative ionization envelope *(left)* and deconvoluted electrospray ionization mass spectrum *(right)* upon incubation of recombinant hCatK for 6 h with excess inhibitor. Covalent adduct is detected by an increase in m/z values and deconvoluted mass (in Da).

Alkynes form a covalent thiovinyl bond with catalytic cysteine residue. Covalent CatK–EM04 adduct was submitted to bottom-up proteomic analysis to identify which amino acid residue is modified. In the tryptic digestion of unreacted CatK, the various length variant peptides containing the NQGQCGSCW-stretch have both Cys22 and Cys25 labeled with a carbamidomethyl group due to the alkylation reaction with iodoacetamide during the sample processing (**Table S2**). After reaction with alkyne EM04, these peptides disappear, but various peptides containing the NQGQCGSCW-stretch appear labeled with one carbamidomethyl group and one inhibitor. Tandem mass spectrometric analysis by HCD and EThcD analysis of peptide NQGQCGSCWAFSSVGALEGQLKKK indicates EM04 is on the second cysteine residue (Cys25; **Table S3**). Together, this clearly shows that one of these cysteine residues is labeled, most likely catalytic Cys25.

The formation of a vinyl thioether linkage between catalytic Cys25 on hCatK and the internal carbon of the alkyne moiety was confirmed by solving the crystal structure of CatK–EM07 adduct (**Figure 6**). Mature CatK was inactivated with MMTS (*S*-methyl methanethiosulfonate) for purification and storage, and reactivated with DTT in the presence of alkyne inhibitors at high concentration (200 μM) to prevent self-degradation of CatK. Solubility of alkynes EM04 and EM05 was not sufficient, which was contributed to the fluoroleucine moiety. We therefore synthesized alkyne EM07 – a closely related derivative in which the fluorine on the ʟ-leucine building block was replaced by a proton to improve solubility (synthesis shown in **Scheme S2**). The resulting CatK–EM07 adduct was crystallized using a sitting drop method, and the structure could be solved at 1.7 Å resolution using maximum-likelihood free-kick (ML FK) electron density map.[42] The refined structure unambiguously revealed the presence of a bond between the thiol atom of Cys25 and the internal carbon in alkyne EM07, with a C–S distance of 1.8 Å (**Figure 6B**).
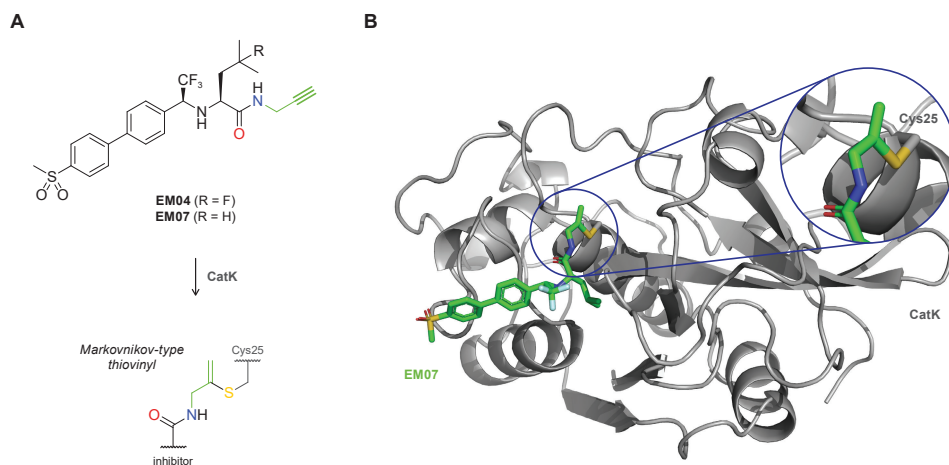

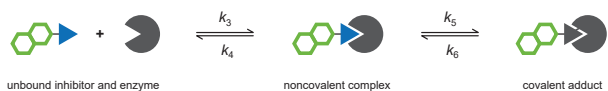**Figure 6 |** Crystal structure of covalent CatK–EM07 adduct. **(A)** Structure of EM07 before and after covalent bond formation with CatK. **(B)** X-ray structure of EM07 bound to catalytic Cys25 in CatK. Coordinates and structure factors for the CatK–EM07 adduct have been submitted to the protein data bank (PDB), accession number 6QBS. Data analysis, refinement statistics and details are provided in **Figure S4**.

Kinetic evaluation. The apparent potency of irreversible covalent inhibitors increases upon longer incubation with the enzyme, since the interaction of inhibitor with enzyme is not at equilibrium.[1, 43-46] As a result, the potency of these compounds can better be assessed by comparison of the k_{inact}/K_I ratio, which can be derived from the progress curve of substrate hydrolysis when the reaction is initiated by addition of the enzyme.[43] Interestingly, the maximum rate of covalent bond formation (k_{inact}) did not correlate with reactivity of the alkyne, as k_{inact} for alkyne EM05 is faster than for electron-deficient alkyne EM06 (**Table 2**). We hypothesize that halogen bonding by the terminal bromine with the thiol moiety on hCatK positions the alkyne less optimal relative to the cysteine residue thus reducing the rate of proximity-driven C–S bond formation.[47] The rate of covalent bond formation for ODN (k_5) is faster than for the alkynes (k_{inact}), also when correcting for the reverse reaction (k_6).

Inhibition of bone resorption activity in osteoclasts. Having established the covalent and irreversible inhibition of CatK on purified recombinant enzyme, we decided to test the inhibitory properties in a biologically relevant setting; inhibition of bone resorption by osteoclasts (OCs). OCs are the cells that degrade the bone matrix by secretion of acid and CatK into the resorption lacunae, resulting in the cleavage of collagen type I (**Figure S6A**). OCs are essential in bone repair, and aberrant activity is observed in numerous diseases including osteoporosis, rheumatoid arthritis, giant cell tumor of the bone, and bone metastases.[48-50]

4

Table 2 | *In vitro* kinetic evaluation of hCatK inhibition.

Irreversible covalent

	k_{inact} ($\times 10^{-3}$ s^{-1})	K_I^{app} (nM)	k_{inact}/K_I ($\times 10^3$ M^{-1}s^{-1})
EM04	0.19 ± 0.012	211 ± 47	0.95 ± 0.22
EM05	0.79 ± 0.061	3255 ± 602	0.26 ± 0.052
EM06	0.32 ± 0.045	193 ± 83	1.8 ± 0.81
E-64	1.3 ± 0.086	11 ± 1.6	N.A.

Reversible covalent

	k_5 ($\times 10^{-3}$ s^{-1})	k_6 ($\times 10^{-3}$ s^{-1})	K_i^{app} (nM)	K_i^* (nM)
ODN	2.0 ± 0.76	0.66	5.7 ± 4.6	0.41 ± 0.071

Activity assay using 100 pM recombinant hCatK and 4 µM fluorogenic substrate Z-FR-AMC. Reaction initialization by addition of CatK. Mean ± SD for a single representative experiment (triplicate measurement). Progress curves and fits are available in **Figure S5**.

Inhibition of osteoclastic CatK was studied by culturing OCs on cortical bone slices in the presence of inhibitor. Mature OCs were obtained by treatment of CD14^{+} monocytes with M-CSF (macrophage colony stimulating factor) and RANKL (receptor activator of nuclear factor κB ligand) to stimulate differentiation to mature OCs (**Figure 7A**).[51] Mature OCs are formed by merging of mononuclear osteoclast precursors to form large multinucleated cells, a process that continued until the end of the culturing period. When the culturing medium was refreshed (every 3 days), inhibitor was freshly added to make sure there always is inhibitor present to inhibit CatK in the newly formed mature OCs. The OCs were cultured on bone slices for sufficient time to clearly observe bone resorption. After culturing for 21 days, the OCs were washed off the bone slices and the resorption pits were stained to visualize bone resorption activity. OCs with normal CatK activity form trenches, resorbing the bone while they move over the surface of the bone. Previously published observations in OCs from CatK^{−/−} mice show that OCs lacking CatK are still able to form shallow pits, but unable to form trenches, with accumulation of collagen I fragments in the lysosomes.[52]

Staining of bone slices for bone resorption showed formation of deep trenches for samples treated with 3 nM ODN, while 15 nM ODN resulted in the formation of shallow pits (**Figure 7B**), corresponding to an effective dose of around 15 nM.[53] Treatment with EM04 successfully inhibited bone resorption at concentrations from 80 nM, while inhibition with EM05 was nonconclusive; we observed trenches as well as pits at all tested concentrations. Quantification of the total resorption area confirmed these observations, even though it is not possible to distinguish between shallow pits and deep trenches (**Figure S6**). From this experiment, we concluded that alkynes EM04 and EM05 inhibit bone resorption with a higher potency than expected based on their potency to inhibit recombinant CatK.

Next, we treated the OC lysates with cathepsin qABP BMV109 to assess whether the observed inhibition of bone resorption could be correlated with CatK activity (**Figure 7C**). CatK activity for OCs treated with DMSO is low, which is expected because mature CatK in its uninhibited form is self-degrading,[54] and the observed bone resorption is the result of secreted mature CatK activity. Additionally, we expect that intracellular CatK is predominantly catalytic inactive proCatK, which is activated by cleavage of the activation peptide, an autoproteolytic event that requires an environment with a low pH for example lysosomes and the resorption lacunae.[55] Interestingly, we observe a strong increase of mature CatK activity in all samples treated with ODN, while samples with EM04 or EM05 do not show any CatK activity. The observed increase in mature CatK activity for ODN-treated samples does not reflect the actual intracellular proteolytic activity, but is the result of displacement of reversibly bound ODN by excess of irreversible qABP BMV109. Alkynes EM04 and EM05 form an irreversible covalent bond with CatK, and can thus not be displaced by BMV109. Western blotting for CatK revealed an increase in the intracellular levels of mature CatK for OCs that were treated with high concentration of any inhibitor, which could be the result of inhibition of proteolytic CatK activity, which would normally degrade mature CatK.

Counting OCs that were cultured on plastic revealed an increase in the number of OCs for the highest concentrations of ODN, EM04 and EM05 (**Figure S7**). This is in agreement with previous reports that observed an increase of OC maturation as a response to CatK activity

loss; the same number of bone marrow cells from CatK^{−/−} mice led to a greater number of active OCs compared to bone marrow cells from the control mice.[52] A significant increase in CatK expression upon 100 nM ODN treatment has been reported, without an increase in the number of OCs.[56] We hypothesize that complete inhibition of CatK activity stimulates the maturation of OCs, and further investigations are advised to identify the feedback mechanism.
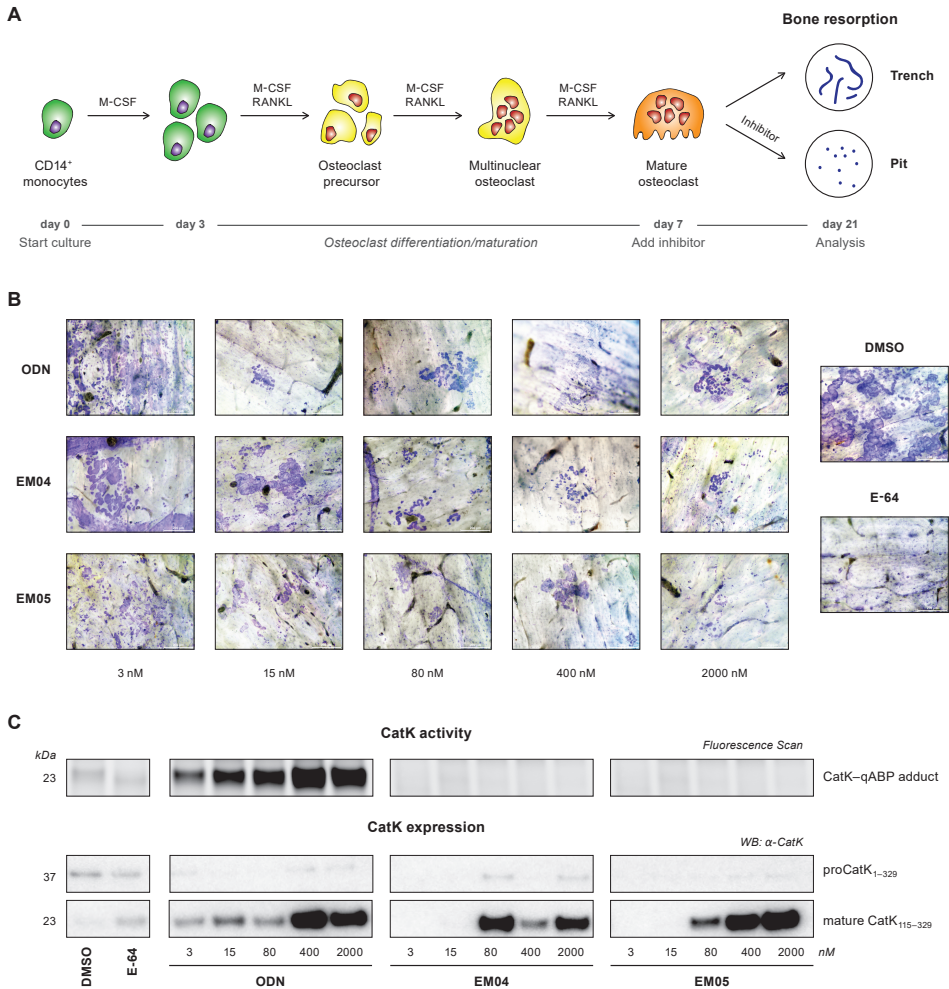

Figure 7 | Inhibition of CatK activity in human osteoclasts (OCs). **(A)** Maturation of OCs from monocytes *(top)* and schematic overview of cellular assay *(bottom)*. CD14^{+} monocytes on bone slices were treated with M-CSF (day 0) and RANKL (day 3) to stimulate differentiation to mature OCs. Medium containing either inhibitor or DMSO was refreshed on day 7, 10, 13, and 16. On day 21, OCs were washed away and lysed, and bone slices were stained to visualize bone resorption. Normal OCs predominantly form deep trenches (paths), while OCs lacking CatK form small pits (circular dots). **(B)** Bone resorption visualized by staining of resorption pits with Coomassie Brilliant Blue. More staining means more resorption pits and, thus, more bone resorption activity. **(C)** CatK activity and expression in OC lysates. *Top:* fluorescence scan of CatK bound to irreversible qABP BMV109 shows mature, active CatK. *Middle/bottom:* Western blotting against CatK shows total amount of CatK present in OC lysates. Darker bands indicate more CatK activity/expression. Full gel scans can be found in **Figure S8**.

3.   Conclusion

To conclude, nonactivated alkynes are not only suitable as latent electrophiles in (large) peptides but also in small molecule inhibitors, as demonstrated here for inhibition of cysteine protease cathepsin K (CatK). Alkyne-based covalent inhibitors do not show indiscriminate thiol reactivity but do form an irreversible covalent bond formation with CatK, as confirmed by MS analysis of intact CatK–inhibitor adducts. X-ray crystallography confirmed the formation of the Markovnikov-type product between the active site cysteine thiol and the internal carbon of the alkyne moiety. Kinetic evaluation shows that the rate of covalent bond formation (k_{inact}) does not correlate with electrophilicity of the alkyne, supporting our hypothesis of proximity-driven reactivity. Optimization of the alkyne position relative to the cysteine residue could result in more potent compounds with faster covalent bond formation while not compromising on indiscriminate thiol reactivity. Treatment of human osteoclasts (OCs) with alkynes EM04 and EM05 showed a potent inhibition of CatK-mediated bone resorption activity, with only a 5-fold difference in effective dose between ODN and EM04. Further investigations into the biological effect of irreversible inhibition of CatK are ongoing.

Finally, we urge everyone using the alkyne moiety as a Click handle to be careful with the assumption that the nonactivated alkyne is truly bioorthogonal; the binding of a small molecule inhibitor can be strong enough to initiate a thiol–alkyne reaction when the alkyne moiety is positioned in close proximity to a cysteine residue. More importantly, based on the proof-of-concept studies described herein, we foresee latent electrophiles such as the alkyne to be of great value in future development of cysteine-targeting covalent inhibitory drugs with a reduced risk of idiosyncratic toxicity.

Competing Interests
The authors declare the following competing financial interest: E.M., H.O., and C.A.A.v.B. are inventors on patent WO2019112426A1, which covers the use of the herein described cathepsin K inhibitors.[57]

Author Contributions
E.M.: Conceptualization, Methodology, Investigation *(Chemical Synthesis, Biochemical Assays)*, Formal Analysis, Writing – Original Draft, Writing – Review & Editing. I.D.C.J.: Investigation *(Cellular Assays)*, Formal Analysis, Writing – Original Draft, Writing – Review & Editing. J.L.: Investigation *(Crystallography)*, Formal Analysis, Writing – Review & Editing. B.R.v.D.: Investigation *(Top-Down MS)*. J.H.: Investigation *(Chemical Synthesis)*. M.V.: Resources, Writing – Review & Editing. C.A.A.v.B.: Conceptualization, Writing – Review & Editing. P.A.v.V.: Investigation *(Bottom-Up MS/MS)*, Formal Analysis. B.T.: Resources, Writing

– Review & Editing. <u>D.T.</u>: Supervision, Writing – Review & Editing. <u>H.O.</u>: Conceptualization, Supervision, Funding Acquisition, Writing – Review & Editing.

4.   Materials and Methods: *Biochemistry*

General

Assay buffers are freshly supplemented with DTT (Chem-Impex, #00127), stored in single-use aliquots at −20 °C (1M aqueous solution). Protease incubations in larger volumes (>50 µL) were performed in Protein Lobind Microtubes (Eppendorf, #022431018) to minimize loss of enzyme and activity. Established irreversible cathepsin inhibitor E-64 (Apollo Sci, #BIMI2157), reversible covalent CatK inhibitor odanacatib (ODN; *in-house* synthesis, see *section 5.2*), thiol-alkylating agent iodoacetamide (IAc; SigmaAldrich, #I6125) were taken along as controls.

4.1.   Indiscriminate Thiol Reactivity

Inhibitor (10 mM in DMSO) was diluted 100-fold in aqueous buffer containing 10 mM cysteine or 5 mM GSH, to a final concentration of 100 µM inhibitor. Aqueous buffers were freshly supplemented with cysteine or GSH, and consisted of PBS pH 7.5 (10 mM phosphate buffer pH7.5, 140 mM NaCl, 2.7 mM KCl), PBS pH 8.0, and MES pH5.5 (50 mM MES pH5.5, 25 mM EDTA). Reaction mixtures were incubated at 37 °C for 23 h under gentle agitation (300 rpm), after which the reaction was quenched by 2-fold dilution in 0.1% FA in 1% DMSO (aq). The samples were submitted to LC-MS analysis as soon as possible, at most 5 h post quenching. Samples were analyzed on the Waters Alliance 2795 Separation Module system equipped with Waters 2996 Photodiode Array Detector (190-750 nm), Waters Xbridge C18 column (2.1×30 mm, 3.5 µm) and LCT ESI- Orthogonal Acceleration Time of Flight Mass Spectrometer. Samples were run with a 13 min gradient using 2 mobile phases: A = 1% MeCN, 0.1% FA in water and B = 1% water and 0.1% FA in MeCN. Data processing was performed using Waters MassLynx Mass Spectrometry Software 4.1. UV trace area was calculated by defining the start and end of the peaks using the 'Edit – integrated peaks' functionality. The intensity of UV signal was determined at a fixed wavelength, corresponding to maximum absorption by the compound and adduct: 265 nm (ODN and analogues), 192 nm (E-64), 260 nm (afatinib/ibrutinib) or 292 nm (acalabrutinib). Adduct formation was quantified from peak integration of the UV trace for the peaks corresponding to the intact compound and thiol adduct, and normalized to 100%. More details can be found in *section 7.2*.

$$\text{Adduct} = 100\% \; \frac{\text{UV}_{\text{adduct}}}{\left(\text{UV}_{\text{adduct}} + \text{UV}_{\text{inhibitor}} \right)}$$

4.2.   *In vitro* Activity Assays (Fluorogenic Substrate Cleavage)

Human recombinant cathepsin K/L/V/S/B for *in vitro* activity assays were prepared as published previously.[58-60] Purified human cathepsins are diluted in freshly prepared reaction buffer (50 mM MES pH5.5, 25 mM EDTA, 2.5 mM DTT), CatK reaction buffers were freshly supplemented with 0.05% Tween20 (v/v). Papain (SigmaAldrich, #P3125) was diluted in freshly prepared reaction buffer consisting of 50 mM Tris pH7.6, 100 mM NaCl, 1 mM DTT, 1 mg/mL CHAPS and 0.5 mg/mL BGG. Controls are E-64 for cathepsins and iodoacetamide for papain. Activity assays were conducted in Corning 3820 Low Volume 384 Well Assay Plate in a final assay volume of 20 µL. Compounds were transferred using an ECHO 550 Liquid Handler (Labcyte Inc) acoustic dispenser. Plates were shaken at 600 rpm for 1 min and centrifuged at 1000 rpm for 1 min prior to incubation. Protease activity was quantified using synthetic fluorogenic peptide substrate: Z-FR-AMC (Bachem, #I-1160), Z-RR-AMC (SigmaAldrich, #C5429), or Z-FVR-AMC. Fluorescence intensity (λ_{ex} = 350 nm, λ_{em} = 440 nm) was measured every 2 min in arbitrary units (A.U.) on a CLARIOstar (BMG Labtech) microplate reader. All measurements were performed in triplicate. Data were plotted and analyzed using GraphPad Prism 8. Graphical data represents the mean ± standard deviation for a single representative experiment.

Potency (IC$_{50}$)

Inhibitors (200 nL, 100× final concentration in DMSO) were dispensed using an ECHO acoustic dispenser and diluted with reaction buffer (10 µL). Purified human cathepsin (5 µL, 4× final concentration, *see below*) was added and the reaction mixture was incubated for 30 min at room temperature. Fluorogenic substrate (5 µL, 4× final concentration, *see below*) was added and fluorescence was measured every 2 min for 90 min. Dose-response curves were calculated from the initial velocity v_i (slope 0-20 min, steady state kinetics), and fitted to obtain IC$_{50}$-values using nonlinear least squares curve fitting (GraphPad Prism: [inhibitor] vs. response – variable slope (four parameters)) with fixed values for the top (DMSO control) and bottom (E-64 for cathepsins; IAc for papain). More details can be found in *section 7.3.*

Protease	[E] (nM)	Fluorogenic substrate	[S] (µM)	K$_M$ (µM)	Ref
hCatK	0.15	Z-FR-AMC	40	48.5	[61]
hCatL	0.005	Z-FR-AMC	4	2.2	[62]
hCatS	1	Z-FVR-AMC	8	8	[62]
hCatV	0.025	Z-FR-AMC	4	4.8	[63]
hCatB	1	Z-RR-AMC	25	173	[64]
Papain	3	Z-FR-AMC	10	420	[65]

Concentrations reported above are final concentrations (after addition of substrate)

Jump Dilution Assay

Recombinant purified CatK (EnzoLifeSci, #BML-SE553-0010) in assay buffer containing 10 mM DTT was activated at 37 °C for 10 min before addition to inhibitor. The plate is mixed (600 rpm, 1 min) and centrifuged (1000 rpm, 1 min). Inhibitors and CatK are preincubated at 37 °C for 40 min, followed by preincubation at 26 °C for 20 min. Then, samples are diluted 300-fold in reaction buffer containing substrate *(jump dilution samples)*, or substrate is added without significant dilution *(control samples)*. The plates are shaken (600 rpm, 26 °C, 1 min) and centrifuged (1000 rpm, 1 min) prior to read-out. The total volume/well and final concentration of CatK and Z-FR-AMC were kept constant between the controls and jump dilution samples. Inhibitor concentrations were selected to correspond to full inhibition prior to dilution (3×IC$_{90}$), and full activity after dilution (IC$_{10}$), which was validated in the control samples without dilution. Positive and negative controls are DMSO and E-64 (19 nM). More details and results can be found in *section 7.4.*

Jump dilution samples. Inhibitor (100 nL) was transferred to a 384-well plate and DMSO (1 µL) was added, followed by CatK (8.9 µL; 120 nM). The reaction mixtures were mixed, centrifuged and preincubated as described above. Then 1 µL was diluted 100-fold in Z-FR-AMC (4 µM), of which 30 µL was diluted 3-fold in Z-FR-AMC (4 µM): final CatK concentration = 0.35 nM. An aliquot (25 µL) was transferred to a 384-well plate for read-out.

Control samples. Inhibitor (2.5-250 nL) was transferred to a 384-well plate with DMSO backfill to 250 nL, and DMSO (2.25 µL) was added, followed by CatK (17.5 µL; 0.5 nM). The reaction mixtures were mixed, centrifuged and preincubated as described above. Then 5 µL Z-FR-AMC (20 µM) was added (final CatK concentration is 0.35 nM) and submitted for read-out.

	ODN	EM04	EM05	EM06
3×IC$_{90}$ = [I] *before* 300-fold dilution	5.6 nM	33 µM	50 µM	5 µM
IC$_{10}$ = [I] *after* 300-fold dilution	0.019 nM	0.11 µM	0.17 µM	0.017 µM

Kinetic Progress Curve Analysis

Inhibitors (200 nL; 100× final concentration in DMSO) were dispensed using an ECHO acoustic dispenser and diluted with reaction buffer (10 µL). Fluorogenic substrate Z-FR-AMC (5 µL; 16 µM, 4× final concentration) was added and the reaction was started by addition of CatK (5 µL; 400 pM, 4× final concentration). Fluorescence intensity was measured every 2 min for 60 min, and data were analyzed using GraphPad Prism 8 to obtain kinetic parameters. Measurements were performed in triplicate (n = 3). Baseline was removed (GraphPad Prism: Remove Baseline and Column Math – Value-Baseline with Baseline = First Row) to give the corrected fluorescence intensity F_t (in RFU). Data analysis was tailored to inhibitor binding mode (as determined in *jump dilution assays*). More details and results can be found in *section 7.7*.

2-step irreversible covalent inhibitors. Time-dependent fluorescence intensity F_t (in RFU) was plotted against incubation time t (in s) for each inhibitor concentration, and the first 60 min were fitted to the one-phase exponential association equation below to find the initial velocity v_i (in RFU/s) and the observed reaction rate constant k_{obs} (in s^{-1}) for time-dependent formation of fluorescent product AMC. The progress curve of the uninhibited DMSO control was also fitted to find k_{ctrl}.

$$F_t = \frac{v_i}{k_{obs}} \left(1 - e^{-k_{obs} t} \right)$$

The means and standard errors of k_{obs} (in s^{-1}) were plotted against inhibitor concentration (in M), and fitted to the equation below to obtain maximum inactivation rate constant k_{inact} (in s^{-1}) and apparent inactivation constant K_I^{app} (in M) in presence of 4 µM Z-FR-AMC. Nonlinearity in uninhibited k_{ctrl} was constrained to the k_{obs} of the uninhibited control.

$$k_{obs} = k_{ctrl} + \frac{k_{inact} [I]}{K_I^{app} + [I]}$$

A correction for substrate competition was performed to obtain inactivation constant K_I (in M) with Gaussian error propagation. The K_M value for hCatK Z-FR-AMC affinity was constrained to the reported $K_M = 48.5$ µM.[61]

$$K_I = \frac{K_I^{app}}{\left(1 + \frac{[S]}{K_M}\right)} \qquad \sigma_{K_I} = \sqrt{\left(\frac{1}{1 + \frac{[S]}{K_M}}\right)^2 \sigma_{K_I^{app}}^2 + \left(-\frac{K_I^{app} K_M}{\left(K_M + [S]\right)^2}\right)^2 \sigma_{[S]}^2 + \left(\frac{K_I^{app} [S]}{\left([S] + K_M\right)^2}\right)^2 \sigma_{K_M}^2}$$

2-step reversible covalent inhibitors. Time-dependent fluorescence intensity F_t (in RFU) was plotted against incubation time t (in s) for each inhibitor concentration, and the first 60 min were fitted to the one-phase exponential association equation below to find the initial velocity v_i (in RFU/s), steady-state velocity v_s (in RFU/s), and the observed reaction rate constant k_{obs} (in s^{-1}) for time-dependent formation of fluorescent product AMC. The progress curve of the uninhibited DMSO control was also fitted to find k_{ctrl} and v_s^{ctrl}.

$$F_t = v_s t + \frac{v_i - v_s}{k_{obs}} \left(1 - e^{-k_{obs} t} \right)$$

The means and standard errors of k_{obs} (in s^{-1}) were plotted against inhibitor concentration (in M), and fitted to the equation below to obtain covalent association rate constant k_5 (in s^{-1}), covalent dissociation rate constant k_6 (in s^{-1}), and apparent inhibition constant K_i^{app} (in M). To obtain stable values, the value for k_6 was constrained to k_{ctrl}.

$$k_{obs} = k_6 + \frac{k_5 [I]}{K_i^{app} + [I]}$$

4

The means and standard errors of steady-state velocity v_s (in RFU/s) were plotted against inhibitor concentration (in M), and fitted to Morrison's quadratic equation with constraints for $[E]_0 = 0.1$ nM, $[S]_0 = 4$ μM, and $K_M = 48.5$ μM to obtain steady-state inhibition constant K_i^* (in M).

$$v_s = v_s^{ctrl} \left[1 - \frac{\left([E]_0 + [I]_0 + K_i^*\left(1 + \frac{[S]}{K_M}\right)\right) - \sqrt{\left([E]_0 + [I]_0 + K_i^*\left(1 + \frac{[S]}{K_M}\right)\right)^2 - 4\,[E]_0\,[I]_0}}{2\,[E]_0} \right]$$

4.3.   Activity Assays with qABP (In-gel Fluorescence)

Recombinant purified CatK (50 nM) in assay buffer (50 mM MES pH5.5, 25 mM EDTA, 2.5 mM DTT, 0.05% Tween20) was incubated with inhibitor (100 μM) for 2 h at 37 °C. Then, quenched fluorescent probe BMV109 (500 nM) was added,[66] and the reaction mixture was incubated at 37 °C for an additional 2 h. The reaction was quenched by addition of loading buffer (3× SDS-PAGE loading buffer, NuPAGE, Invitrogen) containing β-mercaptoethanol as a reducing agent and boiling the samples for 10 min at 94 °C. Samples were loaded on 12% Bis-Tris gels (Invitrogen) and resolved by SDS-PAGE gel electrophoresis with MES (NuPAGE MES SDS running buffer 20×, Novex by Life Technologies) as running buffer. Labeled enzyme was visualized by in-gel fluorescence using Typhoon FLA 9500 imaging system (GE Healthcare Life Sci) ($\lambda_{ex} = 635$ nm, $\lambda_{em} = 665$ nm). Subsequently, gels were stained with InstantBlue™ Ultrafast Protein Stain (Expedeon Protein Solutions) and scanned using an Amersham Imager 600. More details and results can be found in *section 7.3*.

4.4.   MS Analysis of Covalent Adduct

Recombinant purified CatK (~1.5 μM) in reaction buffer (20 μL) was incubated with inhibitor (100 μM) at 37 °C for 6 h to form the covalent adduct prior to MS analysis. Reaction buffer (50 mM MES pH5.5, 25 mM EDTA, 2.5 mM DTT) was not supplemented with Tween20.

Intact protein MS
1 μL injections of the samples containing covalent adduct were made onto a Waters XEVO-G2 XS QTOF UPLC-MS system with a Waters Acquity CM detector. Chromatographic separation was carried out on a Waters ACQUITY UPLC Protein BEH C4 Column (300 Å, 1.7 μm, 2.1×50 mm) over a 12 min gradient elution of 2-100% MeCN in water (0.1% FA) at a flow rate of 0.500 mL/min. For the first 4 min the flow was diverted to the waste to avoid contamination of the MS with high concentrations of buffer components. After 4 min, the gradient was started and the elution flow was ionized with an ESI ionization source in positive ion mode. The data was analyzed using Waters MassLynx Mass Spectrometry Software V4.1. The total mass of the adduct was obtained by deconvolution of electrospray ionization mass spectrum envelope (average isotopes) with the MaxEnt1 function.

Bottom-up MS/MS
Samples containing unbound CatK and preformed CatK–EM04 adduct were run on a 4-12% polyacrylamide gradient gel (NuPAGE Bis-Tris Precast Gel, Life Technologies), and stained with Coomassie protein stain. The CatK band was cut out, and the proteins subjected to reduction with DTT, alkylation with iodoacetamide and in-gel trypsin digestion using Proteineer DP digestion robot (Bruker). Tryptic peptides were extracted from the gel slices, lyophilized, dissolved in 95:3:0.1 water/MeCN/FA (v/v/v) and subsequently analyzed by on-line C18 nanoHPLC MS/MS with a system consisting of an Easy nLC 1200 gradient HPLC system (Thermo, Bremen, Germany), and a LUMOS mass spectrometer (Thermo). Digests were injected onto a homemade precolumn

(100 μm×15 mm; Reprosil-Pur C18-AQ 3 μm, Dr. Maisch, Ammerbuch, Germany) and eluted via a homemade analytical nano-HPLC column (75 μm×15 cm; Reprosil-Pur C18-AQ 3 μm). The gradient was run from 0% to 50% solvent B (20:80:0.1 water/MeCN/FA (v/v/v)) in 20 min. The nano-HPLC column was drawn to a tip of ~5 μm and acted as the electrospray needle of the MS source. The LUMOS mass spectrometer was operated in data-dependent MS/MS (top-10 mode) with collision energy at 32 V and recording of the MS2 spectrum in the orbitrap. In the master scan (MS1) the resolution was 120,000, the scan range 400-1500, at an AGC target of 400,000 @maximum fill time of 50 ms. Dynamic exclusion after n = 1 with exclusion duration of 10 s. Charge states 2-5 were included. For MS2 precursors were isolated with the quadrupole with an isolation width of 1.2 Da. HCD collision energy was set to 32 V. First mass was set to 110 Da. The MS2 scan resolution was 30,000 with an AGC target of 50,000 @maximum fill time of 60 ms. EThcD was performed at an AGC value of 50,000, at a max fill time of 240 ms, and performed with an additional activation of 15 V. Fragment ion spectra were recorded at 120,000 resolution. In a post-analysis process, raw data were first converted to peak lists using Proteome Discoverer version 2.2 (Thermo Electron), and then submitted to the Homo sapiens database (71591 entries), using Mascot v2.2.04 (www.matrixscience.com) for protein identification. Mascot searches were with 10 ppm and 0.02 Da deviation for precursor and fragment mass, respectively, and trypsin as enzyme. Up to four missed cleavages were allowed, and methionine oxidation, and carbamidomethyl on cysteine, and the warhead on cysteine and lysine were set as a variable modification. More details and results can be found in *section 7.5*.

4.5. Protein Crystallography

Expression, purification, and activation of hCatK. *p*PIC9 vector (Invitrogen) carrying cDNA of human procathepsin K (Deutsche Ressourcenzentrum für Genomforschung) was introduced into *P. Pastoris* strain GS115 (Invitrogen) by electroporation. The highest expressing transformant was selected by screening according to Invitrogen *Pichia* Expression kit (Invitrogen, #K1710-01). Large scale expression took place in ten 5L Erlenmeyer flasks of 400 mL of BMMY with the addition of 40 μL antifoam 204 (Sigma, #A8311) per flask, feeding interval 1% MeOH per day and 22 °C for 4 days. The supernatant was then collected, concentrated to 300 mL and diluted at 1:1 ratio with 20 mM HEPES pH7.1. Then 25 mL of SP-sepharose FF (GE Healthcare, #17-079-01) was added to the sample and left shaking overnight at 6 °C. Procathepsin K (proCatK) was eluted from the exchanger with elution buffer (10 mM HEPES pH7.1, 400 mM NaCl), concentrated to 0.5 mg/mL and stored at −80 °C. Activation of proCatK was initiated by adding DTT (5 mM final conc.) to purified proCatK and the sample was diluted at 1:1 ratio with the activation buffer (100 mM NaOAc pH4) containing 40 μg/mL pepsin (Sigma, #P6887) and incubated for 45 min at 37 °C. Pepsin was inactivated by raising pH of the sample to approximately 5.5 with 1M Tris (pH8.5). The sample was then purified on MONO S 5/50 column (GE Healthcare, #17-5168-01) on Äkta Express system (GE Healthcare). Mature hCatK was captured with elution buffer (50 mM NaOAc pH5.5) at approximately 1M NaCl and its proteolytic activity was blocked by incubating with approximately 10-fold molar excess of MMTS (Sigma, #208795) for 20 min at 6 °C. The sample was desalted using HiTrap 5 mL column (GE Healthcare) to the final buffer (50 mM NaOAc pH5.5, 50 mM NaCl) and stored at −80 °C. Active enzyme concentration was determined by titration with E-64 (Sigma, #E3132) based on previously described procedures.[40, 55, 62]

Adduct formation and crystallization of CatK−EM07 adduct. DTT (final conc. 10 mM) and 160 μL of inhibitor EM07 (10 mM stock in DMSO, final inhibitor conc. 200 μM, final conc. DMSO 2%) were added to 8 mL of hCatK (approx. 20 μM) and incubated at 37 °C for 8 h. To ensure complete inhibition, the sample was spiked with DTT (final 3 mM) after 8 h and left incubating for additional 2 h. The adduct was then centrifuged and supernatant was collected and concentrated with Amicon Ultra devices (cut-off 10 kDa) to 15 mg/mL and stored at −80°C. Crystals suitable for data collection grew from 20% PEG-3350, 0.2M CaCl$_2$ at 20 °C with sitting drop method. For the optimization, the adduct was diluted to 10 mg/mL and drop sizes of both precipitant and adduct were varied. Best diffracting crystal grew from the drop consisting of 0.5 μL of adduct and 1 μL of precipitant. The crystal was soaked in 35% PEG-3350, 0.2M CaCl$_2$ for 10 seconds for cryoprotection.

4

Data collection, structure determination, and refinement for X-ray diffraction. Diffraction data was collected at XRD2 beamline at Elettra synchrotron, Trieste[67] under cryogenic conditions. Data were first processed with XDS software,[68] and the unmerged HKL file was used as an input for Pointless, Aimless and Ctruncate (CCP4 suite) [69-71] to obtain the merged MTZ file. The CatK part of the 2FTD model from the Protein Data Bank[72] was used for molecular replacement with Molrep (CCP4 suite).[73] The refinement was done with MAIN software[74] with ML FK target function.[42] Inhibitor EM07 was introduced in the model during refinement and fitted in the difference ML FK map. The geometric restraints for EM07 were generated by PURY.[75] The established adduct was then further refined. Figures were generated in PyMOL v2.2.0. More details and results can be found in *section 7.6*.

4.6. Human Osteoclast Activity

Isolation of CD14+ cells from PBMCs. Osteoclast precursors (CD14+ cells) were isolated from human peripheral blood mononuclear cells (PBMCs). Briefly, human buffy coats were obtained from Sanquin Blood Supply (Amsterdam, NL), diluted 1:1 with PBS containing 1% citrate, and spun down (800 G for 30 min, without brake) in Lymphoprep gradient solution (Elitech). The resulting interphase containing peripheral blood mononuclear cells (PBMCs) was collected and washed with 1% citrate in PBS before it was passed through a 40 µm cell strainer (Greiner Bio-One) to ensure the recovery of a pure mononuclear cell population. The cells were counted on a Muse cell counter (Merck), and cell pellet was resuspended in 80 µL buffer (PBS containing 0.5% BSA and 2 mM EDTA) for 10^7 cells. 20 µL of magnetic MACS CD14 MicroBeads human (Miltenyi Biotec) was added to this cell suspension. According to manufacturer instructions, the cells and CD14 microbeads were mixed and incubated for 15 min at 4 °C. The column was placed in the magnetic field, rinsed and subsequently the cell suspension was applied onto the column. Unlabeled cells pass through. Then the column was removed from the magnet and CD14+ cells were flushed out and collected.

Human osteoclast cultures. Osteoclast precursors (CD14+ cells) were plated in CellStar 96 well plates (Greiner Bio-One) on plastic and on bovine cortical bone slices (650 µm thick) at a density of 1.3×10^6 cells/well. Cells were cultured for 21 days in α-MEM (Gibco, Paisley, UK) supplemented with 5% fetal calf serum (HyClone), 1× antibiotic antimycotic solution containing 100 U/mL penicillin, 100 µg/mL streptomycin and 250 ng/mL amphotericin B (Sigma, #A5955), and 25 ng/mL human recombinant M-CSF (R&D systems). After 3 days, the concentration of M-CSF was reduced to 10 ng/mL and combined with 2 ng/mL recombinant RANKL (R&D systems) until the end of the culture period. From day 7 on, various concentrations of CatK inhibitors were added to the cultures. An equal amount of vehicle (DMSO) was added to the control cultures without inhibitors. During culture the cells were maintained at 37 °C and 5% CO_2 and culture media were refreshed every 3-4 days. After 21 days of culture, wells were washed with PBS and either fixed in 4% PBS buffered formaldehyde, stored at 4 °C, and used for tartrate-resistant acid phosphatase (TRAcP) staining, or the cells were lysed with lysis buffer (100 mM phosphate buffer pH6.0, 0.1% Triton-X100). This cell extract/lysate was stored at −20 °C and used for CatK activity assays in osteoclast lysates. The bone slices were stored in MilliQ water at 4 °C for bone resorption visualization. More details and results can be found in *section 7.8*.

Staining of resorption pits on bone slices. Resorption was measured on slices of bovine cortical bone of 650 µm thick and fit into a 96-well plate. CD14+ monocytes were cultured on these bone slices for 21 days with M-CSF and RANKL and without or with inhibitors in various concentrations, as described above. After this period, the cells present on the bovine cortical bone slices were removed with 0.25M NH_4OH. The slices were washed in distilled water, incubated in a saturated alum ($KAl(SO_4)_2 \cdot 12H_2O$) solution, washed in distilled water, and stained with Coomassie Brilliant Blue. Resorption pits were visualized by light microscopy (Leica DFC320). The resorbed area micrographs were made with 10× magnification. Total resorbed area was quantified using Image Pro Plus (Media Cybernetics) and calculated as a percentage of the total area.

TRAcP staining and cell counting. The cells were stained for TRAcP using the Leukocyte Acid Phosphatase (TRAP) Kit from Sigma (SigmaAldrich, #387A) following manufacturer instructions. Nuclei were visualized with 4'6-diamino-2-phenylindole dihydrochloride (DAPI). Multinucleated TRAcP+ cells with three or more nuclei

were considered osteoclasts and were counted on bone in standardized fields and on plastic per well from a combination of light and fluorescence microscopy using a Leica DFC320 FireWire Digital Microscope Camera (Leica Microsystems).

<u>CatK activity in osteoclast lysates (qABP labeling).</u> Osteoclast lysates (stored at −20 °C and thawed before use) were treated with quenched fluorescent probe BMV109 (1 μM),[66] and the reaction mixture was incubated at 37 °C for 2 h. As a positive control, 5 nM recombinant active hCatK (Enzo Lifesci, #BML-SE553-0010) was also treated with qABP. The reaction was quenched by addition of loading buffer (3× SDS-PAGE loading buffer, NuPAGE, Invitrogen) containing β-mercaptoethanol as a reducing agent and boiling the samples for 10 min at 94 °C. Samples were loaded on 12% Bis-Tris gels (Invitrogen) and resolved by SDS-PAGE gel electrophoresis with MES (NuPAGE MES SDS running buffer 20×, Novex by Life Technologies) as running buffer. Labeled enzyme was visualized by in-gel fluorescence using Typhoon FLA 9500 imaging system (GE Healthcare Life Sci) (λ_{ex} = 635 nm, λ_{em} = 665 nm). Subsequently, gels were stained with InstantBlue Ultrafast Protein Stain (Expedeon Protein Solutions) and scanned on an Amersham Imager 600.

<u>CatK expression in osteoclast lysates (Western blotting).</u> Proteins in osteoclast lysates (stored at −20 °C and thawed before use) were resolved using gel electrophoresis conditions described above. Recombinant mature hCatK (230 ng) and recombinant proCatK (300 ng) were included as references. Gels were transferred to nitrocellulose membrane using a Trans-Blot Turbo Transfer System (Biorad) and subjected to standard Western Blotting protocols. Antibodies: primary rabbit anti-CatK (1:500; Abcam, #19027), primary mouse anti-β-Actin (1:10,000; SigmaAldrich, #A5441), secondary swine anti-rabbit HRP (1:5,000; Dako, #P0217) and secondary goat anti-mouse 800CW (1:5,000; LiCOR, #926-32210). Blots with fluorescent secondary antibodies were scanned on a LiCOR Odyssey system v3.0. Blots with HRP secondary antibody were incubated with SuperSignal West Dura Extended Duration Substrate (Thermo Sci, #34076) according to manufacturer protocols and scanned on an Amersham Imager 600 (chemiluminescence).

4

5.   Materials and Methods: *Chemical Synthesis*

Synthetic schemes can be found in *section 7.1* for precursor carboxylic acid **1**, inhibitor odanacatib (ODN), and odanacatib derivatives EM02-EM06 (**Scheme S1**), for desfluoro precursor **8** and inhibitor EM07 (**Scheme S2**), for building block cyclopropane propargyl **16** for the synthesis of EM03 (**Scheme S3**), and for building block bromoalkyne **19** for the synthesis of EM06 (**Scheme S4**).

General. All commercially available reagents and solvents were used as purchased. Nuclear magnetic resonance (NMR) spectra were recorded on a Bruker Avance 300 (300 MHz for ^{1}H, 75.00 MHz for ^{13}C) using the residual solvent as internal standard ([1]H: δ 7.26 ppm for CDCl$_3$ and 2.50 ppm for DMSO. [13]C: δ 77.16 ppm for CDCl$_3$ and 39.52 ppm for DMSO). Chemical shifts (δ) are given in ppm and coupling constants (*J*) are quoted in hertz (Hz). Resonances are described as s (singlet), d (doublet), t (triplet), q (quartet), b (broad) and m (multiplet) or combinations thereof. Compounds were analyzed using 2D NMR techniques HSQC and HMBC, and coupling constants (J) are reported accordingly. ^{13}C NMR (APT) spectra were obtained to assign C–F coupling constants (*J*) when relevant. Analytical LC-MS analysis was performed on a Waters Alliance 2795 Separation Module system equipped with Waters 2996 Photodiode Array Detector (190-750 nm), Waters Xbridge C18 column (2.1×100 mm, 3.5 μm) and LCT ESI– Orthogonal Acceleration Time of Flight Mass Spectrometer. Samples were run with a 13 min gradient using 2 mobile phases: A = 1% MeCN, 0.1% FA in water and B = 1% water and 0.1% FA in MeCN. Data processing was performed using Waters MassLynx Mass Spectrometry Software 4.1. Electrospray Ionization (ESI) high-resolution mass spectrometry (HRMS) was carried out using a Waters XEVO-G2 XS QTOF UPLC-MS system with a Waters Acquity CM detector in positive ion mode in combination with a Waters Acquity UPLC system equipped with a ACQUITY UPLC Protein BEH C4 Column (300 Å, 1.7 μm, 2.1×50 mm) using water/MeCN mixtures containing 0.1% FA. Thin Layer Chromatography (TLC) was performed using TLC plates from Merck (SiO$_2$, Kieselgel 60 F254 neutral, on aluminum with fluorescence indicator) and compounds were visualized by

UV detection (254 nm) unless mentioned otherwise. Flash column chromatography (FCC) purifications were performed using Grace Davisil Silica Gel (particle size 40-63 µm, pore diameter 60 Å) and the indicated eluent. Reversed phase preparative HPLC/MS was carried out on a Waters AutoPurification system equipped with a Waters 2998 photodiode array detector, Waters 3100 mass detector and a Waters 2767 sample manager using preparative Waters X-bridge C18 column (5 µm, 30 mm×150 mm or 19 mm×150 mm) in combination with water/MeCN mixtures containing 0.1% TFA. Fractions containing the product were automatically collected based on observed mass and UV signals after which they were lyophilized to obtain the pure products. Reported yields are not optimized.

5.1. Synthesis of Precursors 1 and 8

*(4'-bromo-[1,1'-biphenyl]-4-yl)(methyl)sulfane* **9**
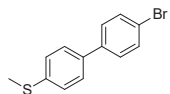
(4-(methylthio)phenyl)boronic acid (3.81 g, 23 mmol), 1-bromo-4-iodobenzene (5.83 g, 21 mmol) and sodium carbonate (6.55 g, 62 mmol) were dissolved in a 4:1 (v/v) DME/water mixture (180 mL). The mixture was degassed with argon for 5 min, then bis(triphenylphosphine)palladium(II) dichloride (579 mg, 0.82 mmol) was added and the mixture was heated to 100 °C. After stirring for 5 hours, the reaction mixture was allowed to cool to room temperature. The reaction was quenched with water and extracted with EtOAc (2X). The combined organic layers were washed with brine (2X), dried over Na_2SO_4, and concentrated under vacuum to give a reddish solid as residue (18.5 g). The crude material was coated on silica and purified by FCC (5% diisopropyl ether in heptane) to give product **9** as a white solid (4.04 g, 14 mmol, 66%). Spectral data was in agreement with published data.[32]

*2,2,2-trifluoro-1-(4'-(methylthio)-[1,1'-biphenyl]-4-yl)ethanone* **10**
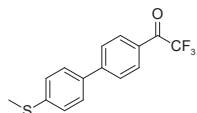
According to published procedure,[32] the reaction of (4'-bromo-[1,1'-biphenyl]-4-yl)(methyl)sulfane **9** (4.04 g, 15 mmol) with ethyl trifluoroacetate (3.44 mL, 29 mmol) and n-BuLi (8.68 mL, 2.5M in hexanes, 22 mmol) afforded product **10** as a light-yellow solid (2.27 g, 7.7 mmol, 53%). Spectral data was in agreement with published data.[32]

2,2,2-trifluoro-1-(4'-(methylsulfonyl)-[1,1'-biphenyl]-4-yl)ethanone **11**
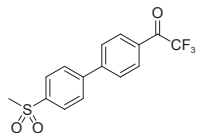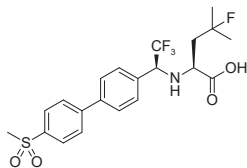

According to published procedure,[32] the reaction between 2,2,2-trifluoro-1-(4'-(methylthio)-[1,1'-biphenyl]-4-yl)ethanone **10** (2.27 g, 7.7 mmol), tetrabutyl-ammonium hydrogen sulfate (130 mg, 0.38 mmol), sodium tungstate dehydrate (126 mg, 0.38 mmol) and 30% aqueous hydrogen peroxide (2.3 mL, 23 mmol) afforded ketone **11** as a white solid (2.42 g). The material was then dehydrated in a Dean-Stark setup by drying the water/toluene azeotrope over molecular sieves. The toluene solution (250 mL) was refluxed overnight. The solution was then cooled to room temperature and concentrated under vacuum to afford ketone **11** as a white crystalline solid (2.30 g, 7.0 mmol, 91%) which was used in the next step. Spectral data was in agreement with published data.[32] ^{1}H NMR (300 MHz, CDCl3) δ 8.19 (ddt, *J* = 8.0, 2.3, 1.1 Hz, 2H), 8.11 – 8.03 (m, 2H), 7.89 – 7.74 (m, 4H), 3.11 (s, 3H). ^{13}C NMR (75 MHz, CDCl3) δ 180.1 (q, *J* = 35.4 Hz), 146.0, 144.7, 140.8, 131.0 (q, *J* = 2.0 Hz), 129.8, 128.5, 128.4, 128.2, 116.7 (q, *J* = 291 Hz), 44.7.

2,2,2-trifluoro-1-(4'-(methylsulfonyl)-[1,1'-biphenyl]-4-yl)ethane-1,1-diol **12**
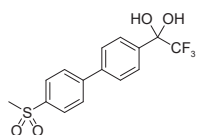
Analysis of ketone **11** in acetone-d_6 or DMSO-d_6 containing trace amounts of water resulted in the (partial) formation of hydrate **12**, which was confirmed by the shift of the CF3 signal from 180.1 ppm to 123.5 ppm in ^{13}C NMR (APT). ^{1}H NMR (300 MHz, DMSO-d_6) δ 8.05 – 7.93 (m, 4H), 7.85 – 7.70 (m, 4H), 7.67 (s, 2H), 3.27 (s, 3H). ^{13}C NMR (75 MHz, DMSO-d_6) δ 144.5, 139.9, 139.0 (d, *J* = 4.6 Hz), 128.3, 127.7, 127.7, 126.7, 123.5 (q, *J* = 289 Hz), 92.5 (q, *J* = 31.2 Hz), 43.6.

(S)-4-fluoro-4-methyl-2-(((S)-2,2,2-trifluoro-1-(4'-(methylsulfonyl)-[1,1'-biphenyl]-4-yl)ethyl)amino)pentanoic acid **(S,S)-1**

According to published procedure,[76] the reaction of ketone **11** (1.23 g, 3.8 mmol) with (S)-ethyl 2-amino-4-fluoro-4-methylpentanoate hydrochloride (1.00 g, 4.7 mmol), potassium carbonate (2.07 g, 15 mmol), and subsequent reduction with zinc chloride (1.02 g, 7.5 mmol) and sodium borohydride (567 mg, 15 mmol) afforded a mixture of desired (S,S)-**1** and (R,S)-**1**, which were separated by preparative RP-HPLC to yield precursor (S,S)-**1** as a white solid (460 mg, 1.0 mmol, 27%). Spectral data of (S,S)-**1** was in agreement with published data.[18] LC-MS Rt = 7.32 min, m/z = 462.11 [M+H]⁺. ¹H NMR (300 MHz, CDCl₃) δ 8.08 – 7.96 (m, 2H), 7.83 – 7.73 (m, 2H), 7.68 – 7.59 (m, 2H), 7.51 (d, *J* = 8.1 Hz, 2H), 4.31 (q, *J* = 7.1 Hz, 1H), 3.68 (dd, *J* = 8.1, 4.1 Hz, 1H), 3.10 (s, 3H), 2.19 (ddd, *J* = 24.8, 15.1, 4.2 Hz, 1H), 1.99 (ddd, *J* = 17.7, 15.0, 8.1 Hz, 1H), 1.48 (d, *J* = 21.8 Hz, 3H), 1.46 (d, *J* = 21.7 Hz, 3H). ¹³C NMR (75 MHz, CDCl₃) δ 175.9, 145.8, 140.6, 139.7, 133.9, 129.4, 128.2, 128.2, 125.3 (q, *J* = 282 Hz), 95.8 (d, *J* = 165 Hz), 62.9 (q, *J* = 29.5 Hz), 56.6, 44.7, 43.6 (d, *J* = 21.5 Hz), 27.5 (d, *J* = 24.3 Hz), 26.8 (d, *J* = 24.4 Hz).

(S)-4-fluoro-4-methyl-2-(((R)-2,2,2-trifluoro-1-(4'-(methylsulfonyl)-[1,1'-biphenyl]-4-yl)ethyl)amino)pentanoic acid **(R,S)-1**
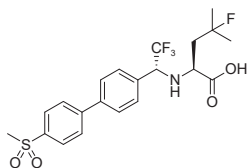
(R,S)-**1** was obtained as the minor isomer in above described synthesis. LC-MS Rt = 7.04 min, m/z = 462.11 [M+H]⁺. ¹H NMR (300 MHz, CDCl₃) δ 8.08 – 7.99 (m, 2H), 7.82 – 7.73 (m, 2H), 7.67 (d, *J* = 8.2 Hz, 2H), 7.52 (d, *J* = 7.9 Hz, 2H), 4.12 (q, *J* = 7.1 Hz, 1H), 3.47 – 3.37 (m, 1H), 3.11 (s, 3H), 2.15 – 1.91 (m, 2H), 1.39 (d, *J* = 22.1 Hz, 3H), 1.15 (d, *J* = 21.6 Hz, 3H). ¹³C NMR (75 MHz, CDCl₃) δ 174.5, 145.6, 140.7, 139.8, 133.0, 129.7, 128.2, 128.1, 124.7 (q, *J* = 281 Hz), 96.5 (d, *J* = 164 Hz), 63.5 (q, *J* = 29.6 Hz), 56.7, 44.8, 43.1 (d, *J* = 20.2 Hz), 28.3 (d, *J* = 24.3 Hz), 25.5 (d, *J* = 24.5 Hz).

(2S)-4-Methyl-2-[(1S)-2,2,2-trifluoro-1-(4'-methanesulfonyl-biphenyl-4-yl)-ethylamino]-pentanoic acid **(S,S)-8**
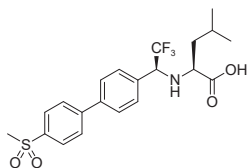
According to published procedure,[76] the reaction of ketone **11** (484 mg, 1.5 mmol) with L-Leucine methyl ester hydrochloride (307 mg, 1.7 mmol), potassium carbonate (749 mg, 5.4 mmol), and subsequent reduction with zinc chloride (371 mg, 2.7 mmol) and sodium borohydride (207 mg, 5.5 mmol) afforded a mixture of (S,S)-**8** and (R,S)-**8**, which could be separated by preparative RP-HPLC to yield the major isomer (S,S)-**8** as a white solid (93.9 mg, 0.21 mmol, 14%). Spectral data of (S,S)-**8** was in agreement with published data.[77] LC-MS Rt = 7.68 min, m/z = 444.14 [M+H]⁺. ¹H NMR (300 MHz, CDCl₃) δ 8.06 – 7.96 (m, 2H), 7.81 – 7.69 (m, 2H), 7.68 – 7.58 (m, 2H), 7.52 (d, *J* = 8.1 Hz, 2H), 4.18 (q, *J* = 7.0 Hz, 1H), 3.58 (dd, *J* = 8.7, 5.3 Hz, 1H), 3.10 (s, 3H), 1.93 (dp, *J* = 13.4, 6.5 Hz, 1H), 1.67 – 1.41 (m, 2H), 0.97 (d, *J* = 6.5 Hz, 3H), 0.95 (d, *J* = 6.7 Hz, 3H). ¹³C NMR (75 MHz, CDCl₃) δ 180.3, 145.9, 140.1, 139.6, 135.2, 129.2, 128.1, 128.1, 127.9, 126.0 (q, *J* = 282 Hz), 63.2 (q, *J* = 29.2 Hz), 58.6, 44.7, 42.7, 24.9, 23.0, 21.8.

((R)-2,2,2-trifluoro-1-(4'-(methylsulfonyl)-[1,1'-biphenyl]-4-yl)ethyl)-L-leucine **(R,S)-8**
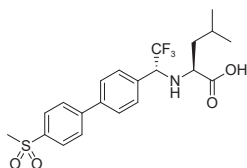
(R,S)-**8** was obtained as the minor isomer in above described synthesis. LC-MS Rt = 7.42 min, m/z = 444.14 [M+H]⁺. ¹H NMR (300 MHz, CDCl₃) δ 8.11 – 7.95 (m, 2H), 7.90 – 7.73 (m, 2H), 7.71 – 7.61 (m, 2H), 7.56 (d, *J* = 8.1 Hz, 2H), 4.31 (q, *J* = 7.1 Hz, 1H), 3.18 – 3.12 (m, 1H), 3.11 (s, 3H), 1.97 – 1.77 (m, 1H), 1.54 (t, *J* = 7.1 Hz, 2H), 0.92 (d, *J* = 6.6 Hz, 3H), 0.76 (d, *J* = 6.5 Hz, 3H). ¹³C NMR (75 MHz, CDCl₃) δ 178.7, 145.9, 140.5, 139.7, 133.6, 130.0, 128.2, 128.2, 127.9, 124.9 (q, *J* = 281 Hz), 63.0 (q, *J* = 29.1 Hz), 56.4, 44.8, 42.9, 24.7, 23.2, 21.7.

4

5.2. Synthesis of Odanacatib Derivatives

General Procedure A: Amide coupling with HATU/DIPEA in DMAc

Adjustment of reported procedure.[78] Precursor (S,S)-**1** (60 mg, 0.13 mmol) was dissolved in 3 mL DMAc and cooled to 0 °C. Amine (0.16 mmol) and HATU (59 mg, 0.16 mmol) were added. The resulting solution was stirred for 15 min and DIPEA (68 mL, 0.39 mmol) was added. The reaction was stirred for 2.5 h. Water was slowly added dropwise and the slurry was stirred 2.5 h at room temperature. The mixture was filtered and the solid material was washed with a 1:1.2 DMF/water solution, with water, and with 2-propanol. The material was removed from the filter by addition of THF. The filtrate was concentrated and purified by FCC (gradient 0-2% MeOH in DCM). The product was obtained as a white solid.

General Procedure B: Amide coupling with HATU/Et$_3$N in DMF

Adjustment of reported procedure.[33] Precursor (S,S)-**1** (21.3 mg, 0.046 mmol) was dissolved in 400 µL DMF and cooled to 0 °C. HATU (21.8 mg, 0.057 mmol) and triethylamine (6 µL, 0.043 mmol) were added. To this solution was added to amine (0.067 mmol) and further triethylamine (12 µL, 0.086 mmol) was added to the mixture. After 2 h, ice cooling was removed and the mixture was stirred an additional 2 h. The reaction mixture was concentrated *in vacuo*, redissolved in EtOAc and extracted with saturated NH$_4$Cl solution (aq) and brine. The organic layer was dried over Na$_2$SO$_4$ and filtered. The filtrate was concentrated *in vacuo* and the residue was purified by FCC (gradient 0-2% MeOH in DCM), and if needed, further purified using Reversed phase preparative HPLC/MS and lyophilized to obtain product as a white solid.

(S)-N-(1-cyanocyclopropyl)-4-fluoro-4-methyl-2-(((S)-2,2,2-trifluoro-1-(4'-(methylsulfonyl)-[1,1'-biphenyl]-4-yl) ethyl)amino)pentanamide **ODN**
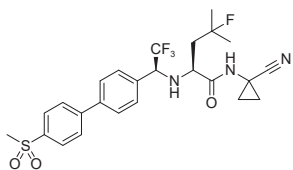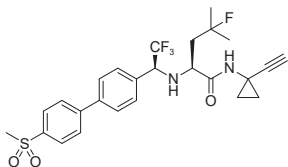

According to *general procedure A*, the reaction between precursor (S,S)-**1** (59.8 mg, 0.13 mmol) and 1-amino-cyclopropanecarbonitrile hydrochloride (18.5 mg, 0.16 mmol) afforded product **ODN** as a white solid (40.7 mg, 0.077 mmol, 60%). TLC Rf = 0.18 (1:1 EtOAc/heptane). LC-MS Rt = 7.43 min, m/z = 526.112 [M+H]$^+$. ^{1}H NMR (300 MHz, CDCl$_3$) δ 8.03 (d, *J* = 8.4 Hz, 2H), 7.77 (d, *J* = 8.8 Hz, 2H), 7.65 (d, *J* = 8.1 Hz, 2H), 7.48 (d, *J* = 8.1 Hz, 2H), 7.42 (s, 1H), 4.17 (q, *J* = 7.2 Hz, 1H), 3.59 (dd, *J* = 8.9, 3.3 Hz, 1H), 3.10 (s, 3H), 2.17 – 1.85 (m, 2H), 1.56 – 1.44 (m, 2H), 1.47 (d, *J* = 21.7 Hz, 3H), 1.44 (d, *J* = 22.0 Hz, 3H), 1.11 – 0.85 (m, 2H). ^{13}C NMR (75 MHz, CDCl$_3$) δ 174.4, 145.7, 140.6, 139.9, 134.5, 129.4, 128.2, 128.2, 126.0 (q, *J* = 279 Hz), 119.6, 96.8 (d, *J* = 164 Hz), 63.4 (q, *J* = 29.3 Hz), 59.0, 44.8, 43.6 (d, *J* = 19.9 Hz), 28.4 (d, *J* = 24.4 Hz), 25.8 (d, *J* = 24.7 Hz), 20.2, 16.9, 16.5. HRMS (ESI$^+$): calculated for C$_{25}$H$_{28}$F$_4$N$_3$O$_3$S [M+H]$^+$ 526.1788, found: 526.1816.

(S)-N-(cyanomethyl)-4-fluoro-4-methyl-2-(((S)-2,2,2-trifluoro-1-(4'-(methylsulfonyl)-[1,1'-biphenyl]-4-yl)ethyl) amino)pentanamide **EM02**
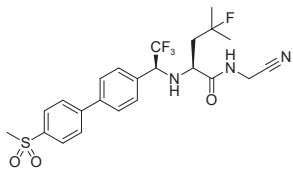
According to *general procedure B*, the reaction between precursor (S,S)-**1** (21.3 mg, 0.046 mmol) and aminoacetonitrile (6.2 mg, 0.067 mmol) afforded product **EM02** as a white solid (15.3 mg, 0.030 mmol, 66%). TLC Rf = 0.15 (1:1 EtOAc/heptane). LC-MS Rt = 7.30 min, m/z = 500.144 [M+H]$^+$. ^{1}H NMR (300 MHz, CDCl$_3$) δ 8.01 (d, *J* = 8.4 Hz, 2H), 7.76 (d, *J* = 8.4 Hz, 2H), 7.65 (d, *J* = 8.4 Hz, 2H), 7.50 (d, *J* = 8.2 Hz, 2H), 7.45 (t, *J* = 6.7 Hz, 1H), 4.24 (q, *J* = 7.1 Hz, 1H), 4.21 – 3.96 (m, 2H), 3.66 (dd, *J* = 8.8, 3.3 Hz, 1H), 3.10 (s, 3H), 2.21 – 1.89 (m, 2H), 1.47 (d, *J* = 21.7 Hz, 3H), 1.45 (d, *J* = 22.0 Hz, 3H). ^{13}C NMR (75 MHz, CDCl$_3$) δ 173.8, 145.7, 140.5, 139.7, 134.2, 129.4, 128.2, 128.2, 125.4 (q, *J* = 283 Hz), 115.7, 96.8 (d, *J* = 164 Hz), 63.1 (q, *J* = 28.7 Hz), 58.5, 44.7, 43.6 (d, *J* = 19.9 Hz), 28.4 (d, *J* = 24.2 Hz), 27.3, 25.7 (d, *J* = 24.7 Hz). HRMS (ESI$^+$): calculated for C$_{23}$H$_{26}$F$_4$N$_3$O$_3$S [M+H]$^+$ 500.1631, found: 500.1638.

*(S)-N-(1-ethynylcyclopropyl)-4-fluoro-4-methyl-2-(((S)-2,2,2-trifluoro-1-(4'-(methylsulfonyl)-[1,1'-biphenyl]-4-yl)ethyl)amino)pentanamide* **EM03**
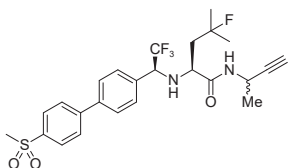
According to *general procedure A*, the reaction between precursor (S,S)-**1** (60.7 mg, 0.13 mmol) and 1-ethynylcyclopropan-1-amine hydrochloride **16** (18.3 mg, 0.16 mmol) afforded product **EM03** as a white solid (46.6 mg, 0.089 mmol, 68%). TLC Rf = 0.24 (1:1 EtOAc/heptane). LC-MS Rt = 7.66 min, m/z = 525.124 [M+H]$^+$. ^{1}H NMR (300 MHz, CDCl$_3$) δ 8.02 (d, J = 8.5 Hz, 2H), 7.76 (d, J = 8.4 Hz, 2H), 7.62 (d, J = 8.3 Hz, 2H), 7.47 (d, J = 8.1 Hz, 2H), 7.32 (s, 1H), 4.14 (q, J = 7.2 Hz, 1H), 3.58 (dd, J = 9.0, 3.2 Hz, 1H), 3.10 (s, 3H), 2.94 (s, 1H), 2.10 (s, 1H), 2.19 − 1.84 (m, 2H), 1.46 (d, J = 21.7 Hz, 6H), 1.43 (d, J = 22.0 Hz, 6H), 1.27 − 1.07 (m, 2H), 0.95 − 0.86 (m, 1H), 0.75 − 0.66 (m, 1H). ^{13}C NMR (75 MHz, CDCl$_3$) δ 173.9, 145.8, 140.2, 139.7, 135.0, 129.3, 128.2, 128.0, 125.5 (q, J = 283 Hz), 97.0 (d, J = 163 Hz), 84.7, 67.0, 63.0 (q, J = 28.8 Hz), 59.2, 44.7, 43.6 (d, J = 19.9 Hz), 28.4 (d, J = 24.3 Hz), 25.7 (d, J = 24.7 Hz), 22.5, 17.7, 17.2. HRMS (ESI$^+$): calculated for C$_{26}$H$_{29}$F$_4$N$_2$O$_3$S [M+H]$^+$ 525.1835, found: 525.1824.

(S)-4-fluoro-4-methyl-N-(prop-2-yn-1-yl)-2-(((S)-2,2,2-trifluoro-1-(4'-(methylsulfonyl)-[1,1'-biphenyl]-4-yl)ethyl)amino)pentanamide **EM04**
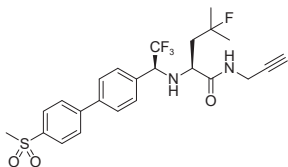
According to *general procedure B*, the reaction between precursor (S,S)-**1** (20.6 mg, 0.045 mmol) and propargylamine (10 µL, 0.16 mmol) afforded product **EM04** as a white solid (11.3 mg, 0.023 mmol, 51%). TLC Rf = 0.25 (1:1 EtOAc/heptane). LC-MS Rt = 7.50 min, m/z = 499.116 [M+H]$^+$. ^{1}H NMR (300 MHz, CDCl$_3$) δ 8.02 (d, J = 8.5 Hz, 2H), 7.76 (d, J = 8.6 Hz, 2H), 7.63 (d, J = 8.4 Hz, 2H), 7.51 (d, J = 8.1 Hz, 2H), 7.22 (t, J = 5.5 Hz, 1H), 4.23 (q, J = 7.2 Hz, 1H), 3.94 (qdd, J = 17.6, 5.5, 2.6 Hz, 2H), 3.69 (dd, J = 9.2, 3.1 Hz, 1H), 3.42 (s, 1H), 3.10 (s, 3H), 2.18 (t, J = 2.6 Hz, 1H), 2.14 − 1.89 (m, 2H), 1.48 (d, J = 21.7 Hz, 3H), 1.45 (d, J = 22.0 Hz, 3H). ^{13}C NMR (75 MHz, CDCl$_3$) δ 173.8, 145.9, 140.3, 139.7, 134.6, 129.4, 128.2, 128.0, 125.5 (q, J = 283 Hz), 97.0 (d, J = 164 Hz), 78.9, 71.9, 63.0 (q, J = 28.7 Hz), 58.7, 44.7, 43.7 (d, J = 19.8 Hz), 29.2, 28.6 (d, J = 24.5 Hz), 25.5 (d, J = 24.8 Hz). HRMS (ESI$^+$): calculated for C$_{24}$H$_{27}$F$_4$N$_2$O$_3$S [M+H]$^+$ 499.1679, found: 499.1713.

(S)-N-((R/S)-but-3-yn-2-yl)-4-fluoro-4-methyl-2-(((S)-2,2,2-trifluoro-1-(4'-(methylsulfonyl)-[1,1'-biphenyl]-4-yl)ethyl)amino)pentanamide **EM05**

According to *general procedure B*, the reaction between precursor (S,S)-**1** (19.9 mg, 0.043 mmol) and 1-methyl-prop-2-ynylamine hydrochloride (16.5 mg, 0.16 mmol) afforded an inseparable 1:1 mixture of diastereo-isomers (S,S,R)-**EM05** and (S,S,S)-**EM05** as a white solid (10.0 mg, 0.020 mmol, 45%). Reported ppm-values are average values. TLC Rf = 0.31 (1:1 EtOAc/heptane). LC-MS Rt = 7.77 min, m/z = 513.130 [M+H]$^+$. ^{1}H NMR (300 MHz, CDCl$_3$) δ 8.02 (d, J = 8.6 Hz, 2H), 7.76 (d, J = 8.6 Hz, 2H), 7.63 (d, J = 8.3 Hz, 2H), 7.51 (d, J = 8.2 Hz, 2H), 7.21 (d, J = 8.3 Hz, 1H), 4.74 − 4.58 (m, 1H), 4.20 (q, J = 14.5 Hz, 1H), 3.68 (t, J = 7.7 Hz, 1H), 3.60 (s, 1H), 3.10 (s, 3H), 2.20 (d, J = 9.0 Hz, 1H), 2.16 − 1.86 (m, 2H), 1.47 (dd, J = 22.0, 10.0 Hz, 6H), 1.24 (d, J = 6.9 Hz, 3H). ^{13}C NMR (75 MHz, CDCl$_3$) δ 173.0, 145.9, 140.2, 139.7, 134.8, 129.4, 128.1, 125.5 (q, J = 284 Hz), 97.1 (d, J = 163 Hz), 83.4, 70.8, 63.0 (q, J = 28.6 Hz), 59.0, 44.7, 43.7 (d, J = 19.8 Hz), 36.9, 28.6 (d, J = 24.3 Hz), 25.4 (d, J = 24.7 Hz), 22.0. HRMS (ESI$^+$): calculated for C$_{25}$H$_{29}$F$_4$N$_2$O$_3$S [M+H]$^+$ 513.1835, found: 513.1829.

4

(S)-N-(3-bromoprop-2-yn-1-yl)-4-fluoro-4-methyl-2-(((S)-2,2,2-trifluoro-1-(4'-(methylsulfonyl)-[1,1'-biphenyl]-4-yl)ethyl)amino)pentanamide **EM06**
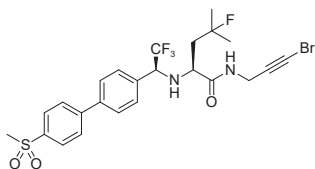
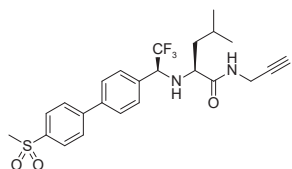According to *general procedure A*, the reaction between precursor (S,S)-**1** (60.8 mg, 0.13 mmol) and 3-bromoprop-2-yn-1-amine hydrochloride **19** (26.6 mg, 0.16 mmol) afforded product **EM06** as a white solid (13.6 mg, 0.024 mmol, 18%). TLC Rf = 0.33 (1:1 EtOAc/heptane). LC-MS Rt = 7.93 min, m/z = 577.036 & 579.038 [M+H]$^+$. ^{1}H NMR (300 MHz, CDCl$_3$) δ 8.03 (d, *J* = 8.4 Hz, 2H), 7.78 (d, *J* = 8.4 Hz, 2H), 7.65 (d, *J* = 8.2 Hz, 2H), 7.50 (d, *J* = 8.1 Hz, 2H), 7.16 (t, *J* = 5.3 Hz, 1H), 4.21 (q, *J* = 7.2 Hz, 1H), 4.13 − 3.81 (m, 2H), 3.68 (dd, *J* = 9.2, 3.1 Hz, 1H), 3.11 (s, 3H), 2.20 − 1.88 (m, 3H), 1.49 (d, *J* = 21.7 Hz, 6H), 1.45 (d, *J* = 22.0 Hz, 6H). ^{13}C NMR (75 MHz, CDCl$_3$) δ 173.1, 145.9, 140.2, 139.7, 134.8, 129.4, 128.2, 128.1, 128.0, 125.6 (q, *J* = 284 Hz), 97.0 (d, *J* = 163 Hz), 75.5, 62.9 (q, *J* = 28.6 Hz), 58.9, 44.7, 43.8 (d, *J* = 19.9 Hz), 43.2, 30.0, 28.6 (d, *J* = 24.4 Hz), 25.5 (d, *J* = 24.7 Hz). HRMS (ESI$^+$): calculated for C$_{24}$H$_{26}$BrF$_4$N$_2$O$_3$S [M+H]$^+$ 577.0784, found: 577.0809 (minor) & 579.0781 (major).

(S)-4-methyl-N-(prop-2-yn-1-yl)-2-(((S)-2,2,2-trifluoro-1-(4'-(methylsulfonyl)-[1,1'-biphenyl]-4-yl)ethyl)amino) pentanamide **EM07**

According to *general procedure B*, the reaction between precursor (S,S)-**8** (26.9 mg, 0.06 mmol) and propargylamine (14 µL, 0.22 mmol) afforded product **EM07** as a white solid (10.1 mg, 0.02 mmol, 35%). TLC Rf = 0.13 (1:2 EtOAc/heptane). LC-MS Rt = 8.41 min, m/z = 481.01 [M+H]$^+$. ^{1}H NMR (300 MHz, CDCl$_3$) δ 8.05 − 7.99 (m, 2H), 7.79 − 7.73 (m, 2H), 7.65 − 7.59 (m, 2H), 7.51 (d, *J* = 8.1 Hz, 2H), 6.87 (t, *J* = 5.4 Hz, 1H), 4.20 (q, *J* = 7.2 Hz, 1H), 4.05 − 3.84 (m, 2H), 3.43 (dd, *J* = 8.9, 4.7 Hz, 1H), 3.11 (s, 3H), 2.19 (t, *J* = 2.6 Hz, 1H), 1.81 (tt, *J* = 12.8, 6.4 Hz, 1H), 1.69 − 1.42 (m, 2H), 0.97 (d, *J* = 6.5 Hz, 3H), 0.96 (d, *J* = 6.6 Hz, 3H). ^{13}C NMR (75 MHz, CDCl$_3$) δ 174.4, 145.9, 140.3, 139.7, 134.6, 129.4, 128.2, 128.0, 125.5 (q, *J* = 283 Hz), 79.1, 71.9, 63.4 (q, *J* = 28.7 Hz), 59.8, 44.8, 43.0, 29.2, 25.0, 23.3, 21.9.

5.3. Synthesis of Alkyne 16

tert-butyl (1-(methoxy(methyl)carbamoyl)cyclopropyl)carbamate **13**

A solution of 1-(Boc-amino)cyclopropanecarboxylic acid (200 mg, 0.99 mmol) in DCM (2.5 mL) under argon was cooled to −15 °C. *N,O*-Dimethylhydroxylamine hydrochloride (100 mg, 1.0 mmol) was added, followed by 4-methylmorpholine (113 mL, 1.0 mmol). After 5 min, 1-(3-methylaminopropyl-3-ethylcarbodiimide hydrochloride (195 mg, 1.0 mmol) was added and the reaction was allowed to reach room temperature and stirred overnight. Water was added and the solution was extracted with DCM (3X). The combined organic phases were washed with brine, dried over Na$_2$SO$_4$, and concentrated *in vacuo* to obtain pure Weinreb amide **13** as an off-white solid (1.08 g, 0.99 mmol, quantitative). TLC Rf = 0.35 (1:1 EtOAc/heptane). ^{1}H NMR (300 MHz, CDCl$_3$) δ 5.22 (s, 1H), 3.74 (s, 3H), 3.18 (s, 3H), 1.44 (q, *J* = 5.2 Hz, 2H), 1.44 (s, 9H), 1.03 (q, *J* = 4.8 Hz, 2H). ^{13}C NMR (75 MHz, DMSO-*d*$_6$) δ 171.9, 155.3, 78.0, 60.6, 34.0, 28.2, 21.2, 14.7.

tert-butyl (1-formylcyclopropyl)carbamate **14**

Tert-butyl (1-(methoxy(methyl)carbamoyl)cyclopropyl) carbamate **13** (500 mg, 2.3 mmol) was dissolved in anhydrous Et$_2$O (50 mL) under argon and cooled to 0 °C. Lithium Aluminum Hydride (3.0 mL, 1M in Et$_2$O, 3.0 mmol) was added dropwise and the reaction mixture was stirred for 2 h at this temperature. The reaction was quenched by addition of 1N HCl (2.5 mL) and stirred vigorously for a few minutes. The organic layer was extracted with 1N HCl and brine, dried over Na$_2$SO$_4$, filtered and concentrated to obtain the product aldehyde **14** as a colorless oil. Use crude in the next step. TLC Rf = 0.47 (1:1 EtOAc/heptane).

tert-butyl (1-ethynylcyclopropyl)carbamate **15**
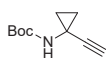
Dimethyl (1-diazo-2-oxopropyl)phosphonate (443 mL, 2.8 mmol) was dissolved in MeCN (25 mL) and potassium carbonate (767 mg, 5.6 mmol) was added. The suspension was stirred at room temperature for 10 min, then the freshly prepared aldehyde **14** (428 mg, 2.3 mmol) in MeOH (9 mL) was added. Stirring was continued overnight. The solvents were removed *in vacuo* and the residue was dissolved in 1:1 Et$_2$O/water. The layers were separated and the organic layer was washed with water and brine, and dried over Na$_2$SO$_4$. The yellowish oil was purified by FCC (1:2 EtOAc/heptane) to give product **15** as a pale white solid (165 mg, 0.90 mmol, 39%). TLC Rf = 0.66 (1:1 EtOAc/heptane). ^{1}H NMR (300 MHz, CDCl$_3$) δ 5.00 (s, 1H), 2.13 (s, 1H), 1.46 (s, 9H), 1.23 – 1.16 (m, 2H), 1.12 – 1.01 (m, 2H). ^{13}C NMR (75 MHz, CDCl$_3$) δ 155.5, 85.8, 80.3, 66.8, 28.5, 23.7, 18.1.

1-ethynylcyclopropan-1-amine hydrochloride **16**
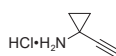
To a solution of *tert*-butyl (3-bromoprop-2-yn-1-yl)carbamate **15** (165 mg, 0.91 mmol) in MeOH (4.5 mL) was added 1.25N HCl in MeOH (1.82 mL, 2.3 mmol). The reaction mixture was left to stir overnight, volatiles were removed *in vacuo* and the resulting solid was triturated with Et$_2$O to obtain alkyne **16** as a white solid (79 mg, 0.67 mmol, 74%). ^{1}H NMR (300 MHz, DMSO-*d$_6$*) δ 8.74 (s, 3H), 3.59 (s, 1H), 1.26 (m, 2H), 1.23 – 1.07 (m, 2H). ^{13}C NMR (75 MHz, DMSO-*d$_6$*) δ 81.8, 74.4, 23.9, 13.7.

5.4.   Synthesis of Alkyne 19

tert-butyl prop-2-yn-1-ylcarbamate **17**
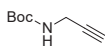
According to published procedure,[79] the reaction between 3-amino-1-propyne (3.2 mL, 50 mmol) and di-*tert*-butyl dicarbonate (10.9 g, 50 mmol) afforded product **17** (7.8 g, 50 mmol, quantitative) as a yellow solid. TLC Rf = 0.78 (1:1 EtOAc/heptane). ^{1}H NMR (300 MHz, CDCl$_3$) δ 4.92 (s, 1H), 3.86 (dd, *J* = 5.9, 2.5 Hz, 2H), 2.18 (t, *J* = 2.5 Hz, 1H), 1.40 (s, 9H). ^{13}C NMR (75 MHz, CDCl$_3$) δ 155.4, 80.2, 80.0, 71.2, 30.4, 28.4.

tert-butyl (3-bromoprop-2-yn-1-yl)carbamate **18**
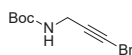
Tert-butyl prop-2-yn-1-ylcarbamate **17** (583 mg, 3.8 mmol) was dissolved in 19 mL DMF and silver nitrate (64 mg, 0.38 mmol) was added, followed by the addition of *N*-bromosuccinimide (735 mg, 4.1 mmol, 1.1 eq). The mixture was covered with aluminum foil and stirred at room temperature for 2 h, and was diluted with EtOAc and extracted with water (2X). The combined organic layers were dried over Na$_2$SO$_4$, filtered over celite and concentrated to give a yellow solid. The crude material was purified by FCC (3:1-2:1 EtOAc in heptane) to give bromoalkyne **18** (618 mg, 2.64 mmol, 70%) as an off-white solid. TLC Rf = 0.58 (1:2 EtOAc/heptane). ^{1}H NMR (300 MHz, CDCl$_3$) δ 4.69 (s, 1H), 3.94 (d, *J* = 5.5 Hz, 2H), 1.45 (s, 9H). ^{13}C NMR (75 MHz, CDCl$_3$) δ 155.3, 80.2, 76.5, 42.8, 31.5, 28.4.

3-bromoprop-2-yn-1-amine hydrochloride **19**
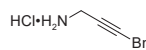
To *tert*-butyl (3-bromoprop-2-yn-1-yl)carbamate **18** (69 mg, 0.29 mmol) was added 4N HCl in dioxane (2 mL, 8 mmol). The reaction mixture was left to stir 1 h, volatiles were removed *in vacuo* and the resulting solid was triturated with Et$_2$O to obtain product **19** (51.4 mg, 0.32 mmol, quantitative) as a white solid. ^{1}H NMR (300 MHz, DMSO-*d$_6$*) δ 8.58 (s, 3H), 3.75 (s, 2H). ^{13}C NMR (75 MHz, DMSO-*d$_6$*) δ 73.5, 48.9, 29.2.

6.   References

1.   Singh, J.; Petter, R.C.; Baillie, T.A.; Whitty, A. The Resurgence of Covalent Drugs. *Nat. Rev. Drug Discov.* **2011**, *10*, 307-317. doi: 10.1038/nrd3410.

2.   Bauer, R.A. Covalent Inhibitors in Drug Discovery: From Accidental Discoveries To Avoided Liabilities and Designed Therapies. *Drug Discov. Today* **2015**, *20*, 1061-1073. doi: 10.1016/j.drudis.2015.05.005.

3.   Silva, D.G.; Ribeiro, J.F.R.; De Vita, D.; Cianni, L.; Franco, C.H.; Freitas-Junior, L.H.; Moraes, C.B.; Rocha, J.R.; Burtoloso, A.C.B.; Kenny, P.W.; Leitão, A.; Montanari, C.A. A Comparative Study of Warheads for Design of Cysteine Protease Inhibitors. *Bioorg. Med. Chem. Lett.* **2017**, *27*, 5031-5035. doi: 10.1016/j.bmcl.2017.10.002.

4.   Lonsdale, R.; Burgess, J.; Colclough, N.; Davies, N.L.; Lenz, E.M.; Orton, A.L.; Ward, R.A. Expanding the Armory: Predicting and Tuning Covalent Warhead Reactivity. *J. Chem. Inf. Model.* **2017**, *57*, 3124-3137. doi: 10.1021/acs.jcim.7b00553.

5.   Barf, T.; Kaptein, A. Irreversible Protein Kinase Inhibitors: Balancing the Benefits and Risks. *J. Med. Chem.* **2012**, *55*, 6243-6262. doi: 10.1021/jm3003203.

6.   Baillie, T.A. Targeted Covalent Inhibitors for Drug Design. *Angew. Chem. Int. Ed.* **2016**, *55*, 13408-13421. doi: 10.1002/anie.201601091.

7.   González-Bello, C. Designing Irreversible Inhibitors—Worth the Effort? *ChemMedChem* **2015**, *11*, 22-30. doi: 10.1002/cmdc.201500469.

8.   Solca, F.; Dahl, G.; Zoephel, A.; Bader, G.; Sanderson, M.; Klein, C.; Kraemer, O.; Himmelsbach, F.; Haaksma, E.; Adolf, G.R. Target Binding Properties and Cellular Activity of Afatinib (BIBW 2992), an Irreversible ErbB Family Blocker. *J. Pharmacol. Exp. Ther.* **2012**, *343*, 342-350. doi: 10.1124/jpet.112.197756.

9.   Pan, Z.; Scheerens, H.; Li, S.-J.; Schultz, B.E.; Sprengeler, P.A.; Burrill, L.C.; Mendonca, R.V.; Sweeney, M.D.; Scott, K.C.K.; Grothaus, P.G.; Jeffery, D.A.; Spoerke, J.M.; Honigberg, L.A.; Young, P.R.; Dalrymple, S.A.; Palmer, J.T. Discovery of Selective Irreversible Inhibitors for Bruton's Tyrosine Kinase. *ChemMedChem* **2006**, *2*, 58-61. doi: 10.1002/cmdc.200600021.

10.   Liu, Q.; Sabnis, Y.; Zhao, Z.; Zhang, T.; Buhrlage, S.J.; Jones, L.H.; Gray, N.S. Developing Irreversible Inhibitors of the Protein Kinase Cysteinome. *Chem. Biol.* **2013**, *20*, 146-159. doi: 10.1016/j.chembiol.2012.12.006.

11.   Shibata, Y.; Chiba, M. The Role of Extrahepatic Metabolism in the Pharmacokinetics of the Targeted Covalent Inhibitors Afatinib, Ibrutinib, and Neratinib. *Drug Metab. Dispos.* **2015**, *43*, 375.

12.   Nakayama, S.; Atsumi, R.; Takakusa, H.; Kobayashi, Y.; Kurihara, A.; Nagai, Y.; Nakai, D.; Okazaki, O. A Zone Classification System for Risk Assessment of Idiosyncratic Drug Toxicity Using Daily Dose and Covalent Binding. *Drug Metab. Dispos.* **2009**, *37*, 1970. doi: 10.1124/dmd.109.027797.

13.   Schwöbel, J.A.H.; Koleva, Y.K.; Enoch, S.J.; Bajot, F.; Hewitt, M.; Madden, J.C.; Roberts, D.W.; Schultz, T.W.; Cronin, M.T.D. Measurement and Estimation of Electrophilic Reactivity for Predictive Toxicology. *Chem. Rev.* **2011**, *111*, 2562-2596. doi: 10.1021/cr100098n.

14.   Zhao, Z.; Bourne, P.E. Progress with Covalent Small-Molecule Kinase Inhibitors. *Drug Discov. Today* **2018**, *23*, 727-735. doi: 10.1016/j.drudis.2018.01.035.

15.   Wright, M.H.; Sieber, S.A. Chemical Proteomics Approaches for Identifying the Cellular Targets of Natural Products. *Nat. Prod. Rep.* **2016**, *33*, 681-708. doi: 10.1039/C6NP00001K.

16.   Talele, T.T. Acetylene Group, Friend or Foe in Medicinal Chemistry. *J. Med. Chem.* **2020**, *63*, 5625-5663. doi: 10.1021/acs.jmedchem.9b01617.

17.   Ekkebus, R.; van Kasteren, S.I.; Kulathu, Y.; Scholten, A.; Berlin, I.; Geurink, P.P.; de Jong, A.; Goerdayal, S.; Neefjes, J.; Heck, A.J.R.; Komander, D.; Ovaa, H. On Terminal Alkynes That Can React with Active-Site Cysteine Nucleophiles in Proteases. *J. Am. Chem. Soc.* **2013**, *135*, 2867-2870. doi: 10.1021/ja309802n.

18.   Gauthier, J.Y.; Chauret, N.; Cromlish, W.; Desmarais, S.; Duong, L.T.; Falgueyret, J.-P.; Kimmel, D.B.; Lamontagne, S.; Léger, S.; LeRiche, T.; et al. The Discovery of Odanacatib (MK-0822), a Selective Inhibitor of Cathepsin K. *Bioorg. Med. Chem. Lett.* **2008**, *18*, 923-928. doi: 10.1016/j.bmcl.2007.12.047.

19.   Orlov, N.V. Metal Catalysis in Thiolation and Selenation Reactions of Alkynes Leading to Chalcogen-Substituted Alkenes and Dienes. *ChemistryOpen* **2015**, *4*, 682-697. doi: 10.1002/open.201500137.

20.   Castarlenas, R.; Di Giuseppe, A.; Pérez-Torrente, J.J.; Oro, L.A. The Emergence of Transition-Metal-Mediated Hydrothiolation of Unsaturated Carbon–Carbon Bonds: A Mechanistic Outlook. *Angew. Chem. Int. Ed.* **2012**, *52*, 211-222. doi: 10.1002/anie.201205468.

21.   Lowe, A.B. Thiol-Yne 'Click'/Coupling Chemistry and Recent Applications in Polymer and Materials Synthesis and Modification. *Polymer* **2014**, *55*, 5517-5549. doi: 10.1016/j.polymer.2014.08.015.

22.   Jayasree, E.G.; Reshma, S. A Computational Study on the Reaction Mechanism and Energetics of Markovnikov and Anti-Markovnikov Addition in Alkyne Hydrothiolation Reactions. *Comput. Theor. Chem.* **2016**, *1098*, 13-21. doi: 10.1016/j.comptc.2016.10.012.

23.   Sommer, S.; Weikart, N.D.; Linne, U.; Mootz, H.D. Covalent Inhibition of SUMO and Ubiquitin-Specific Cysteine Proteases by an In Situ Thiol–Alkyne Addition. *Bioorg. Med. Chem.* **2013**, *21*, 2511-2517. doi: 10.1016/j.bmc.2013.02.039.

24.   Arkona, C.; Rademann, J. Propargyl Amides as Irreversible Inhibitors of Cysteine Proteases—A Lesson on the Biological Reactivity of Alkynes. *Angew. Chem. Int. Ed.* **2013**, *52*, 8210-8212. doi: 10.1002/anie.201303544.

25.   Turk, V.; Stoka, V.; Vasiljeva, O.; Renko, M.; Sun, T.; Turk, B.; Turk, D. Cysteine Cathepsins: From Structure, Function and Regulation to New Frontiers. *Biochim. Biophys. Acta, Proteins Proteom.* **2012**, *1824*, 68-88. doi: 10.1016/j.bbapap.2011.10.002.

26.   Vizovišek, M.; Fonović, M.; Turk, B. Cysteine Cathepsins in Extracellular Matrix Remodeling: Extracellular Matrix Degradation and Beyond. *Matrix Biol.* **2019**, *75–76*, 141-159. doi: 10.1016/j.matbio.2018.01.024.

27.   Stoch, S.A.; Zajic, S.; Stone, J.; Miller, D.L.; Van Dyck, K.; Gutierrez, M.J.; De Decker, M.; Liu, L.; Liu, Q.; Scott, B.B.; Panebianco, D.; Jin, B.; Duong, L.T.; Gottesdiener, K.; Wagner, J.A. Effect of the Cathepsin K Inhibitor Odanacatib on Bone Resorption Biomarkers in Healthy Postmenopausal Women: Two Double-Blind, Randomized, Placebo-Controlled Phase I Studies. *Clin. Pharmacol. Ther.* **2009**, *86*, 175-182. doi: 10.1038/clpt.2009.60.

28.   Brömme, D.; Lecaille, F. Cathepsin K Inhibitors for Osteoporosis and Potential Off-Target Effects. *Expert Opin. Invest. Drugs* **2009**, *18*, 585-600. doi: 10.1517/13543780902832661.

29.   Brömme, D.; Panwar, P.; Turan, S. Cathepsin K Osteoporosis Trials, Pycnodysostosis and Mouse Deficiency Models: Commonalities and Differences. *Expert Opin. Drug Discov.* **2016**, *11*, 457-472. doi: 10.1517/17460441.2016.1160884.

30.   Mullard, A. Merck & Co. Drops Osteoporosis Drug Odanacatib. *Nat. Rev. Drug Discov.* **2016**, *15*, 669-669. doi: 10.1038/nrd.2016.207.

31.   Selent, J.; Kaleta, J.; Li, Z.; Lalmanach, G.; Brömme, D. Selective Inhibition of the Collagenase Activity of Cathepsin K. *J. Biol. Chem.* **2007**, *282*, 16492-16501. doi: 10.1074/jbc.M700242200.

32.   Dolman, S.J.; Gosselin, F.; O'Shea, P.D.; Davies, I.W. Selective Metal-Halogen Exchange of 4,4'-Dibromobiphenyl Mediated by Lithium Tributylmagnesiate. *Tetrahedron* **2006**, *62*, 5092-5098. doi: 10.1016/j.tet.2006.03.039.

33. O'Shea, P.D.; Chen, C.-Y.; Gauvreau, D.; Gosselin, F.; Hughes, G.; Nadeau, C.; Volante, R.P. A Practical Enantioselective Synthesis of Odanacatib, a Potent Cathepsin K Inhibitor, via Triflate Displacement of an α-Trifluoromethylbenzyl Triflate. *J. Org. Chem.* **2009**, *74*, 1605-1610. doi: 10.1021/jo8020314.

34. Liu, G.; Kong, L.; Shen, J.; Zhu, G. A Regio- and Stereoselective Entry to (Z)-β-Halo Alkenyl Sulfides and Their Applications to Access Stereodefined Trisubstituted Alkenes. *Org. Biomol. Chem.* **2014**, *12*, 2310-2321. doi: 10.1039/C4OB00103F.

35. Shiu, H.-Y.; Chan, T.-C.; Ho, C.-M.; Liu, Y.; Wong, M.-K.; Che, C.-M. Electron-Deficient Alkynes as Cleavable Reagents for the Modification of Cysteine-Containing Peptides in Aqueous Medium. *Chem. Eur. J.* **2009**, *15*, 3839-3850. doi: 10.1002/chem.200800669.

36. Barf, T.; Covey, T.; Izumi, R.; van de Kar, B.; Gulrajani, M.; van Lith, B.; van Hoek, M.; de Zwart, E.; Mittag, D.; Demont, D.; Verkaik, S.; Krantz, F.; Pearson, P.G.; Ulrich, R.; Kaptein, A. Acalabrutinib (ACP-196): A Covalent Bruton Tyrosine Kinase Inhibitor with a Differentiated Selectivity and In Vivo Potency Profile. *J. Pharmacol. Exp. Ther.* **2017**, *363*, 240. doi: 10.1124/jpet.117.242909.

37. Oballa, R.M.; Truchon, J.-F.; Bayly, C.I.; Chauret, N.; Day, S.; Crane, S.; Berthelette, C. A Generally Applicable Method for Assessing the Electrophilicity and Reactivity of Diverse Nitrile-Containing Compounds. *Bioorg. Med. Chem. Lett.* **2007**, *17*, 998-1002. doi: 10.1016/j.bmcl.2006.11.044.

38. Siklos, M.; BenAissa, M.; Thatcher, G.R.J. Cysteine Proteases as Therapeutic Targets: Does Selectivity Matter? A Systematic Review of Calpain and Cathepsin Inhibitors. *Acta Pharm. Sin. B* **2015**, *5*, 506-519. doi: 10.1016/j.apsb.2015.08.001.

39. Lushchak, V.I. Glutathione Homeostasis and Functions: Potential Targets for Medical Interventions. *J. Amino Acids* **2012**, *2012*, 736837. doi: 10.1155/2012/736837.

40. Law, S.; Andrault, P.-M.; Aguda, A.H.; Nguyen, N.T.; Kruglyak, N.; Brayer, G.D.; Brömme, D. Identification of Mouse Cathepsin K Structural Elements that Regulate the Potency of Odanacatib. *Biochem. J.* **2017**, *474*, 851-864. doi: 10.1042/BCJ20160985.

41. Copeland, R.A.; Basavapathruni, A.; Moyer, M.; Scott, M.P. Impact of Enzyme Concentration and Residence Time on Apparent Activity Recovery in Jump Dilution Analysis. *Anal. Biochem.* **2011**, *416*, 206-210. doi: 10.1016/j.ab.2011.05.029.

42. Pražnikar, J.; Turk, D. Free Kick Instead of Cross-Validation in Maximum-Likelihood Refinement of Macromolecular Crystal Structures. *Acta Crystallogr., Sect. D: Biol. Crystallogr.* **2014**, *70*, 3124-3134. doi: 10.1107/S1399004714021336.

43. Strelow, J.M. A Perspective on the Kinetics of Covalent and Irreversible Inhibition. *SLAS Discov.: Adv. Life Sci. R&D* **2017**, *22*, 3-20. doi: 10.1177/1087057116671509.

44. Holdgate, G.A.; Meek, T.D.; Grimley, R.L. Mechanistic Enzymology in Drug Discovery: A Fresh Perspective. *Nat. Rev. Drug Discov.* **2017**, *17*, 115. doi: 10.1038/nrd.2017.219.

45. Strelow, J.M.; Dewe, W.; Iversen, P.W.; Brooks, H.B.; Radding, J.A.; McGee, J.; Weidner, J. Mechanism of Action Assays for Enzymes. In *Assay Guidance Manual* [Online], Eli Lilly & Company and the National Center for Advancing Translational Sciences: Bethesda (MD), 2012. https://www.ncbi.nlm.nih.gov/books/NBK92001/ (accessed 2012-10-01).

46. Copeland, R.A. Chapter 9. Irreversible Enzyme Inactivators. In *Evaluation of Enzyme Inhibitors in Drug Discovery: A Guide for Medicinal Chemists and Pharmacologists*, Second ed.; John Wiley & Sons, Inc.: Hoboken, New Jersey, 2013; pp 345-382. doi: 10.1002/9781118540398.

47. Cavallo, G.; Metrangolo, P.; Milani, R.; Pilati, T.; Priimagi, A.; Resnati, G.; Terraneo, G. The Halogen Bond. *Chem. Rev.* **2016**, *116*, 2478-2601. doi: 10.1021/acs.chemrev.5b00484.

48. Drake, M.T.; Clarke, B.L.; Oursler, M.J.; Khosla, S. Cathepsin K Inhibitors for Osteoporosis: Biology, Potential Clinical Utility, and Lessons Learned. *Endocr. Rev.* **2017**, *38*, 325-350. doi: 10.1210/er.2015-1114.

49. Lindeman, J.H.N.; Hanemaaijer, R.; Mulder, A.; Dijkstra, P.D.S.; Szuhai, K.; Bromme, D.; Verheijen, J.H.; Hogendoorn, P.C.W. Cathepsin K Is the Principal Protease in Giant Cell Tumor of Bone. *Am. J. Pathol.* **2004**, *165*, 593-600. doi: 10.1016/S0002-9440(10)63323-8.

50. Edgington-Mitchell, L.E.; Rautela, J.; Duivenvoorden, H.M.; Jayatilleke, K.M.; van der Linden, W.A.; Verdoes, M.; Bogyo, M.; Parker, B.S. Cysteine Cathepsin Activity Suppresses Osteoclastogenesis of Myeloid-Derived Suppressor Cells in Breast Cancer. *Oncotarget* **2015**, *6*, 27008-27022. doi: 10.18632/oncotarget.4714.

51. Nicholson, G.C.; Malakellis, M.; Collier, F.M.; Cameron, P.U.; Holloway, W.R.; Gough, T.J.; Gregorio-King, C.; Kirkland, M.A.; Myers, D.E. Induction of Osteoclasts from CD14-Positive Human Peripheral Blood Mononuclear Cells by Receptor Activator of Nuclear Factor κB Ligand (RANKL). *Clin. Sci.* **2000**, *99*, 133. doi: 10.1042/cs0990133.

52. Kiviranta, R.; Morko, J.; Alatalo, S. L.; NicAmhlaoibh, R.; Risteli, J.; Laitala-Leinonen, T.; Vuorio, E. Impaired Bone Resorption in Cathepsin K-Deficient Mice is Partially Compensated for by Enhanced Osteoclastogenesis and Increased Expression of Other Proteases via an Increased RANKL/OPG Ratio. *Bone* **2005**, *36*, 159-172. doi: 10.1016/j.bone.2004.09.020.

53. Pirapaharan, D.C.; Søe, K.; Panwar, P.; Madsen, J.S.; Bergmann, M.L.; Overgaard, M.; Brömme, D.; Delaisse, J.-M. A Mild Inhibition of Cathepsin K Paradoxically Stimulates the Resorptive Activity of Osteoclasts in Culture. *Calcif. Tissue Int.* **2019**, *104*, 92-101. doi: 10.1007/s00223-018-0472-7.

54. Thompson, S.K.; Halbert, S.M.; Bossard, M.J.; Tomaszek, T.A.; Levy, M.A.; Zhao, B.; Smith, W.W.; Abdel-Meguid, S.S.; Janson, C.A.; D'Alessio, K.J., et al. Design of Potent and Selective Human Cathepsin K Inhibitors That Span the Active Site. *Proc. Natl. Acad. Sci.* **1997**, *94*, 14249. doi: 10.1073/pnas.94.26.14249.

55. McQueney, M.S.; Amegadzie, B.Y.; D'Alessio, K.; Hanning, C.R.; McLaughlin, M.M.; McNulty, D.; Carr, S.A.; Ijames, C.; Kurdyla, J.; Jones, C.S. Autocatalytic Activation of Human Cathepsin K. *J. Biol. Chem.* **1997**, *272*, 13955-13960. doi: 10.1074/jbc.272.21.13955.

56. Leung, P.; Pickarski, M.; Zhuo, Y.; Masarachia, P.J.; Duong, L.T. The Effects of the Cathepsin K Inhibitor Odanacatib on Osteoclastic Bone Resorption and Vesicular Trafficking. *Bone* **2011**, *49*, 623-635. doi: 10.1016/j.bone.2011.06.014.

57. Ovaa, H.; Mons, M.W.E.; van Boeckel, S. Cathepsin Inhibitors. WO2019112426A1, 13 June, 2019.

58. Mihelič, M.; Doberšek, A.; Gunčar, G.; Turk, D. Inhibitory Fragment from the p41 Form of Invariant Chain Can Regulate Activity of Cysteine Cathepsins in Antigen Presentation. *J. Biol. Chem.* **2008**, *283*, 14453-14460. doi: 10.1074/jbc.M801283200.

59. Brömme, D.; Nallaseth, F.S.; Turk, B. Production and Activation of Recombinant Papain-Like Cysteine Proteases. *Methods* **2004**, *32*, 199-206. doi: 10.1016/S1046-2023(03)00212-3.

60. Rozman, J.; Stojan, J.; Kuhelj, R.; Turk, V.; Turk, B. Autocatalytic Processing of Recombinant Human Procathepsin B Is a Bimolecular Process. *FEBS Lett.* **1999**, *459*, 358-362. doi: 10.1016/S0014-5793(99)01302-2.

61. Choe, Y.; Leonetti, F.; Greenbaum, D.C.; Lecaille, F.; Bogyo, M.; Brömme, D.; Ellman, J.A.; Craik, C.S. Substrate Profiling of Cysteine Proteases Using a Combinatorial Peptide Library Identifies Functionally Unique Specificities. *J. Biol. Chem.* **2006**, *281*, 12824-12832. doi: 10.1074/jbc.M513331200.

62. Borišek, J.; Vizovišek, M.; Sosnowski, P.; Turk, B.; Turk, D.; Mohar, B.; Novič, M. Development of *N*-(Functionalized benzoyl)-homocycloleucyl-glycinonitriles as Potent Cathepsin K Inhibitors. *J. Med. Chem.* **2015**, *58*, 6928-6937. doi: 10.1021/acs.jmedchem.5b00746.

63. Yasuda, Y.; Li, Z.; Greenbaum, D.; Bogyo, M.; Weber, E.; Brömme, D. Cathepsin V, a Novel and Potent Elastolytic Activity Expressed in Activated Macrophages. *J. Biol. Chem.* **2004**, *279*, 36761-36770. doi: 10.1074/jbc.M403986200.

4

64. Kramer, L.; Renko, M.; Završnik, J.; Turk, D.; Seeger, M.A.; Vasiljeva, O.; Grütter, M.G.; Turk, V.; Turk, B. Non-invasive *In Vivo* Imaging of Tumour-Associated Cathepsin B by a Highly Selective Inhibitory DARPin. *Theranostics* **2017**, *7*, 2806-2821. doi: 10.7150/thno.19081.

65. Menard, R.; Khouri, H.E.; Plouffe, C.; Dupras, R.; Ripoll, D.; Vernet, T.; Tessier, D.C.; Laliberte, F.; Thomas, D.Y.; Storer, A.C. A Protein Engineering Study of the Role of Aspartate 158 in the Catalytic Mechanism of Papain. *Biochemistry* **1990**, *29*, 6706-6713. doi: 10.1021/bi00480a021.

66. Verdoes, M.; Oresic Bender, K.; Segal, E.; van der Linden, W.A.; Syed, S.; Withana, N.P.; Sanman, L.E.; Bogyo, M. Improved Quenched Fluorescent Probe for Imaging of Cysteine Cathepsin Activity. *J. Am. Chem. Soc.* **2013**, *135*, 14726-14730. doi: 10.1021/ja4056068.

67. Lausi, A.; Polentarutti, M.; Onesti, S.; Plaisier, J.R.; Busetto, E.; Bais, G.; Barba, L.; Cassetta, A.; Campi, G.; Lamba, D.; Pifferi, A.; Mande, S.C.; Sarma, D.D.; Sharma, S.M.; Paolucci, G. Status of the Crystallography Beamlines at Elettra. *Eur. Phys. J. Plus* **2015**, *130*, 43. doi: 10.1140/epjp/i2015-15043-3.

68. Kabsch, W. Integration, Scaling, Space-Group Assignment and Post-Refinement. *Acta Crystallogr., Sect. D* **2010**, *66*, 133-144. doi: 10.1107/S0907444909047374.

69. Winn, M.D.; Ballard, C.C.; Cowtan, K.D.; Dodson, E.J.; Emsley, P.; Evans, P.R.; Keegan, R.M.; Krissinel, E.B.; Leslie, A.G.W.; McCoy, A.; McNicholas, S.J.; Murshudov, G.N.; Pannu, N.S.; Potterton, E.A.; Powell, H.R.; Read, R.J.; Vagin, A.; Wilson, K.S. Overview of the CCP4 Suite and Current Developments. *Acta Crystallogr., Sect. D: Biol. Crystallogr.* **2011**, *67*, 235-242. doi: 10.1107/S0907444910045749.

70. Evans, P. Scaling and Assessment of Data Quality. *Acta Crystallogr., Sect. D* **2006**, *62*, 72-82. doi: 10.1107/S0907444905036693.

71. Evans, P.R.; Murshudov, G.N. How Good are My Data and What Is the Resolution? *Acta Crystallogr., Sect. D: Biol. Crystallogr.* **2013**, *69*, 1204-1214. doi: 10.1107/S0907444913000061.

72. Yamashita, D.S.; Marquis, R.W.; Xie, R.; Nidamarthy, S.D.; Oh, H.-J.; Jeong, J.U.; Erhard, K.F.; Ward, K.W.; Roethke, T.J.; Smith, B.R., et al. Structure Activity Relationships of 5-, 6-, and 7-Methyl-Substituted Azepan-3-one Cathepsin K Inhibitors. *J. Med. Chem.* **2006**, *49*, 1597-1612. doi: 10.1021/jm050915u.

73. Vagin, A.; Teplyakov, A. MOLREP: an Automated Program for Molecular Replacement. *J. Appl. Crystallogr.* **1997**, *30*, 1022-1025. doi: 10.1107/S0021889897006766.

74. Turk, D. MAIN Software for Density Averaging, Model Building, Structure Refinement and Validation. *Acta Crystallogr., Sect. D: Biol. Crystallogr.* **2013**, *69*, 1342-1357. doi: 10.1107/S0907444913008408.

75. Andrejasic, M.; Praznikar, J.; Turk, D. PURY: a Database of Geometric Restraints of Hetero Compounds for Refinement in Complexes with Macromolecular Structures. *Acta Crystallogr., Sect. D* **2008**, *64*, 1093-1109. doi: 10.1107/S0907444908027388.

76. Gauthier, J.Y.; Black, W.C.; Courchesne, I.; Cromlish, W.; Desmarais, S.; Houle, R.; Lamontagne, S.; Li, C.S.; Massé, F.; McKay, D.J.; Ouellet, M.; Robichaud, J.; Truchon, J.-F.; Truong, V.-L.; Wang, Q.; Percival, M.D. The Identification of Potent, Selective, and Bioavailable Cathepsin S Inhibitors. *Bioorg. Med. Chem. Lett.* **2007**, *17*, 4929-4933. doi: 10.1016/j.bmcl.2007.06.023.

77. Roy, A.; Gosselin, F.; O'Shea, P.D.; Chen, C.-Y. Diastereoselective Arylithium Addition to an α-Trifluoromethyl Imine. Practical Synthesis of a Potent Cathepsin K Inhibitor. *J. Org. Chem.* **2006**, *71*, 4320-4323. doi: 10.1021/jo052430j.

78. O'Shea, P.; Gosselin, F. Amidation Process for the Preparation of Cathepsin K Inhibitors. WO2008119176A1, 9 October, 2008.

79. Ishida, T.; Kobayashi, R.; Yamada, T. Novel Method of Tetramic Acid Synthesis: Silver-Catalyzed Carbon Dioxide Incorporation into Propargylic Amine and Intramolecular Rearrangement. *Org. Lett.* **2014**, *16*, 2430-3. doi: 10.1021/ol500806u.

80. Wang, Z. Weinreb Ketone Synthesis. In *Comprehensive Organic Name Reactions and Reagents*, 2010; pp 2963-2967. doi: 10.1002/9780470638859.conrr661.

81. Dhameja, M.; Pandey, J. Bestmann−Ohira Reagent: A Convenient and Promising Reagent in the Chemical World. *Asian J. Org. Chem.* **2018**, *7*, 1502-1523. doi: 10.1002/ajoc.201800051.

82. Halbes-Letinois, U.; Weibel, J.-M.; Pale, P. The Organic Chemistry of Silver Acetylides. *Chem. Soc. Rev.* **2007**, *36*, 759-769. doi: 10.1039/B602151B.

83. Fernández, A.; Vendrell, M. Smart Fluorescent Probes for Imaging Macrophage Activity. *Chem. Soc. Rev.* **2016**, *45*, 1182-1196. doi: 10.1039/C5CS00567A.

84. Rodan, S.B.; Duong, L.T. Cathepsin K – A New Molecular Target for Osteoporosis. *IBMS BoneKEy* **2008**, *5*, 16-24. doi: 10.1138/20080294.

85. Hayman, A.R. Tartrate-Resistant Acid Phosphatase (TRAP) and the Osteoclast/Immune Cell Dichotomy. *Autoimmunity* **2008**, *41*, 218-223. doi: 10.1080/08916930701694667.

7.   Supporting Information

7.1.   Chemical Synthesis
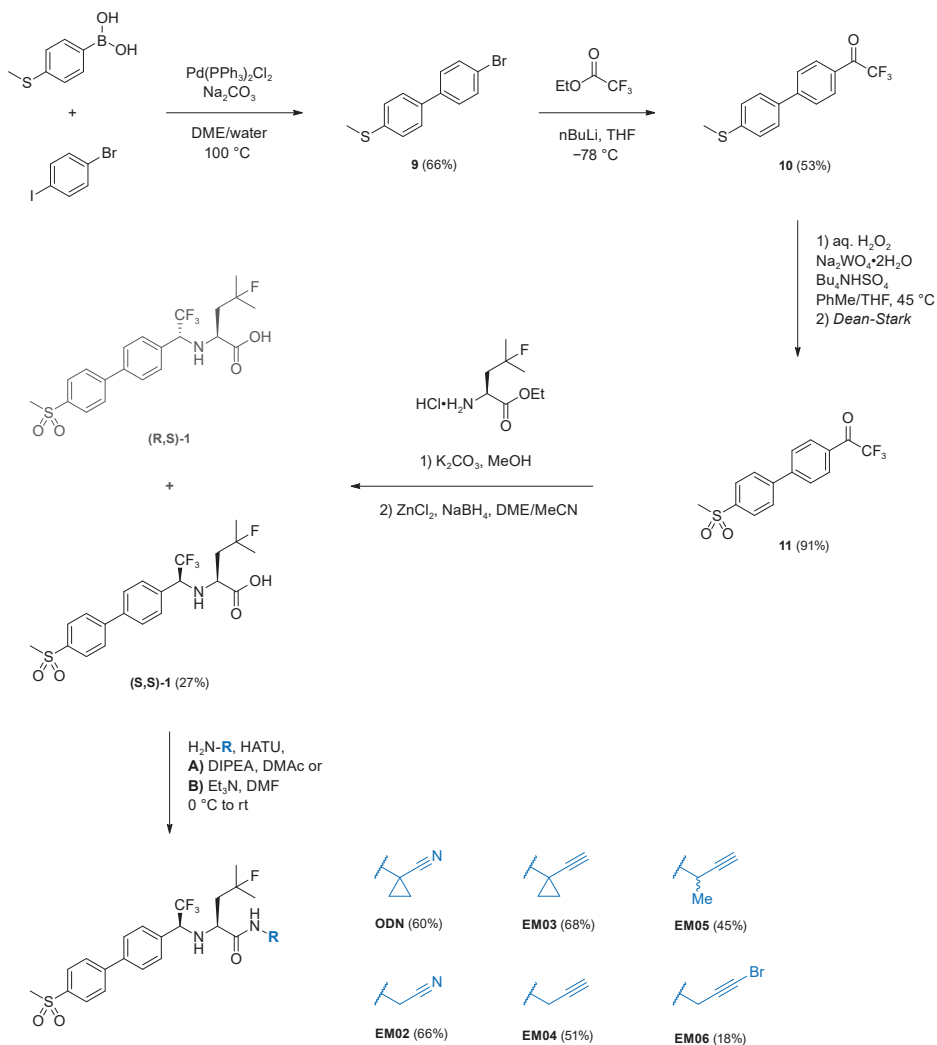
Scheme S1 | Synthesis of ODN and derivatives from affordable building blocks. Synthesis of precursor **1** was started with a Suzuki coupling between commercially available boronic acid and 1-bromo-4-iodobenzene. Obtained product **9** was lithiated in the presence of ethyl trifluoroacetate to give sulfide **10**. Subsequent oxidation resulted in ketone **11**, which is prone to hydrolysis forming hydrate **12**. Ketone **11** was submitted to a diastereoselective reductive amination. The imine intermediate was formed with 4-fluoro-L-leucine, after which it was reduced with NaBH₄/ZnCl₂. Aqueous acidic work-up and purification by flash chromatography resulted in a mixture of diastereoisomers, which could be separated on preparative RP-HPLC. Diastereoisomers (S,S)-**1** and (R,S)-**1** were assigned based on comparison of ¹H NMR to the published spectra of (S,S)-**1**.[33] Ester hydrolysis of both diastereoisomers was also observed. Precursor (S,S)-**1** was then submitted to HATU-catalyzed amide coupling (*conditions A* or *B*) to give the final compounds.
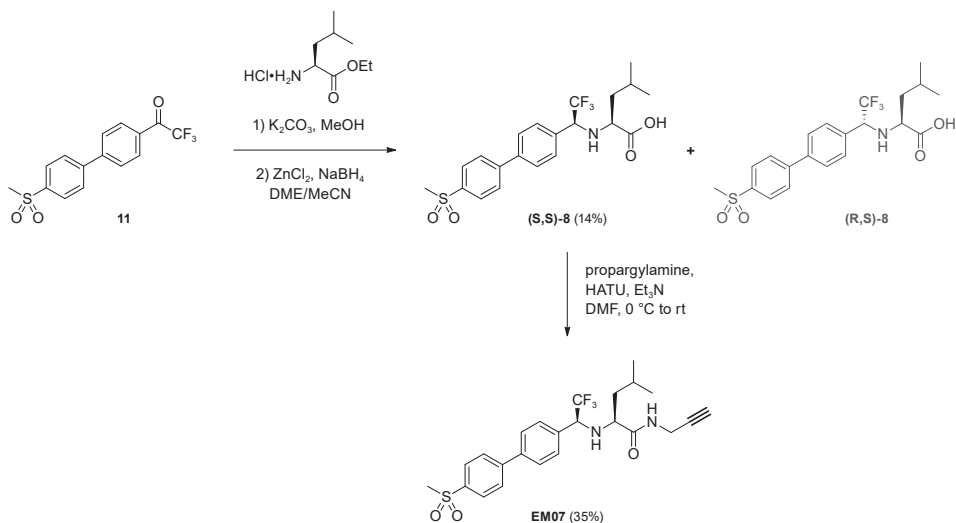
Scheme S2 | Synthesis of **EM07** for crystallography. Ketone **11** was submitted to a diastereoselective reductive amination. The imine intermediate was formed with L-leucine, after which it was reduced with NaBH$_4$/ZnCl$_2$. Aqueous acidic work-up resulted in a mixture of diastereoisomers, which could be separated on preparative RP-HPLC with (S,S)-**8** as the major isomer.[33] Peptide coupling with propargylamine finally resulted in EM07. Stereocenters were assigned based on the X-ray diffraction data of the CatK–EM07 adduct.
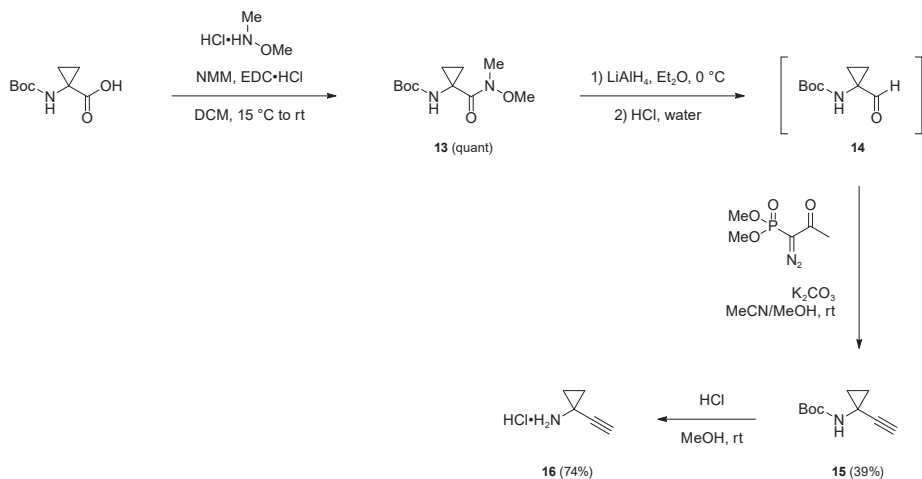
Scheme S3 | Synthesis of building block (cyclopropyl)propargylamine **16**. Treatment of Boc-protected 1-amino-cyclopropanecarboxylic acid with *N,O*-dimethylhydroxylamine in presence of water-soluble coupling reagent EDC formed Weinreb amide **13**,[80] which was obtained pure after a simple aqueous extraction. A reduction in a Weinreb-Nahm ketone synthesis reaction with lithium aluminum hydride followed by aqueous acid treatment formed aldehyde **14**, and solvents were only partially removed *in vacuo* (400 mbar, room temperature) to minimize loss of the volatile product. Crude aldehyde **14** was directly submitted to a Seyferth-Gilbert homologation reaction with Ohira-Bestmann reagent to form Boc-protected alkyne **15**.[81] The Boc-protecting group was removed with HCl to yield the hydrochloride salt of amine **16**.

Scheme S4 | Synthesis of building block bromoalkyne **19**. Installation of a protecting group increases the boiling point (reducing loss of volatile free amine in solvent evaporation steps) and changed the physical appearance from an oil to a solid – greatly improving compound handling – while increasing the molecular weight to above 100 Da facilitates LC-MS detection and NMR analysis. Boc-protected propargylamine **17** was obtained by Boc protection of propargylamine using standard published conditions.[79] Subsequent direct silver-mediated halogenation was achieved by displacement of the terminal alkyne proton of alkyne **17** with silver nitrate to form a silver acetylide intermediate, which reacted with *N*-bromosuccinimide (NBS) to form Boc-protected bromoalkyne **18**.[82] Remnants of unreacted Boc-propargylamine **17** could be removed by flash column chromatography. HCl treatment, removal of solvents *in vacuo* and trituration with Et$_2$O finally yielded the hydrochloride salt of amine **19**.

7.2. Thiol Reactivity Assay

Table S1 | Retention times and m/z for unbound inhibitors and thiol adducts.

Compound	Unbound		Cys adduct		GSH adduct	
	Rt (min)	**m/z**[a]	**Rt** (min)	**m/z**[a]	**Rt** (min)	**m/z**[a]
ODN	7.17	526	6.89 5.94	630 648[b]	N.D.	*833*
EM02	7.04	500	6.69 5.82	604 622[b]	5.68	807
EM03	7.37	525	N.D.	*646*	N.D.	*832*
EM04	7.22	499	5.95	620	5.86	806
EM05	7.45 7.20	513 531[b]	6.08	634	5.84	820
EM06	7.62	577 & 579	6.12	698 & 700	6.04	884 & 886
E-64	3.48	358	2.29	479	2.59 2.80	665 665
afatinib	4.24	486	3.83	607	3.88	793
ibrutinib	6.52	441	5.48	562	5.41 5.21	748 764[b]
acalabrutinib	4.37 3.98	466 484[b]	3.65 3.83	587 587	3.93	773

Data related to **Figure 3**. Detection of unbound inhibitor and adducts by LC-MS, with quantification of UV trace. [a] Values in *italics* are expected/calculated values, not detected. [b] Hydrolysis of inhibitor/adduct. N.D. = not detected.
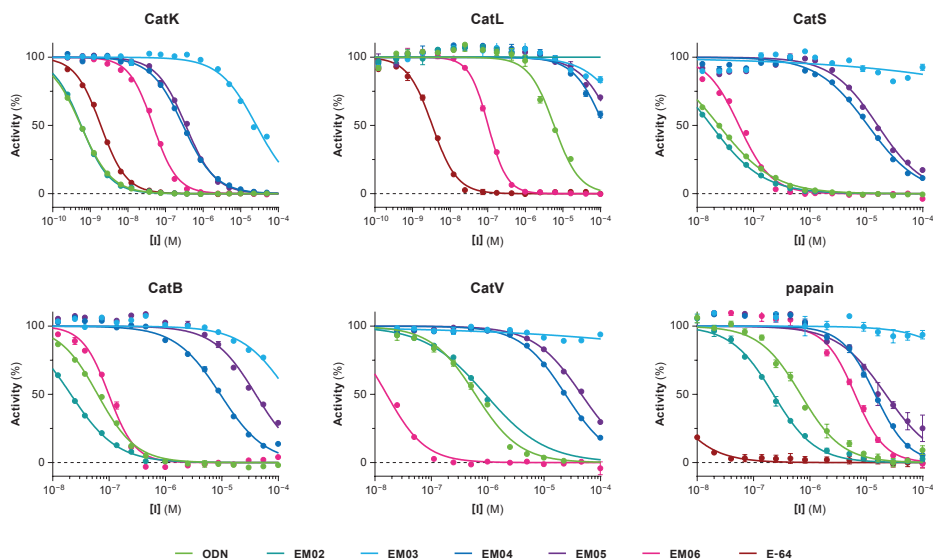
7.3. Activity Assays

Figure S1 | Dose-Response Curves (DRC) for cysteine protease inhibition. Data accompanying **Table 1**. Graphical data represents the mean ± standard deviation for a single representative experiment.
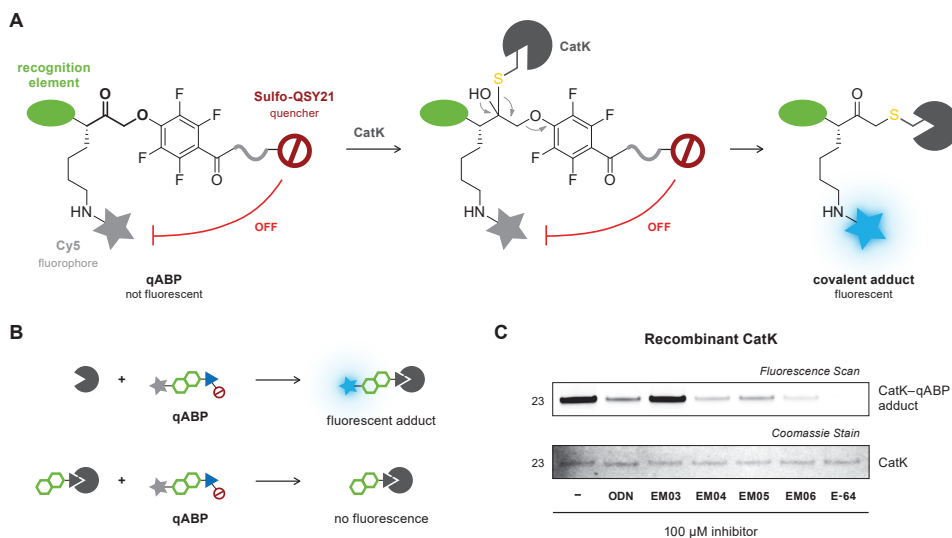

Figure S2 | Evaluation of recombinant hCatK activity with quenched fluorescent ABP (qABP) BMV109. **(A)** Schematic overview.[83] Fluorescent adduct is formed upon covalent thiol addition, with the quencher as leaving group. **(B)** Recombinant CatK is preincubated with inhibitor (2 h) followed by treatment with qABP BMV109 (500 nM) for 2 h. CatK–inhibitor adduct formation blocks formation of fluorescent CatK–qABP adduct.[66] **(C)** Gel electrophoresis results. *Top:* Fluorescence scan (λ_{ex} = 635 nm, λ_{em} = 665 nm) for CatK–qABP adducts. Darker bands = more CatK activity. *Bottom:* Coomassie protein stain as loading control.
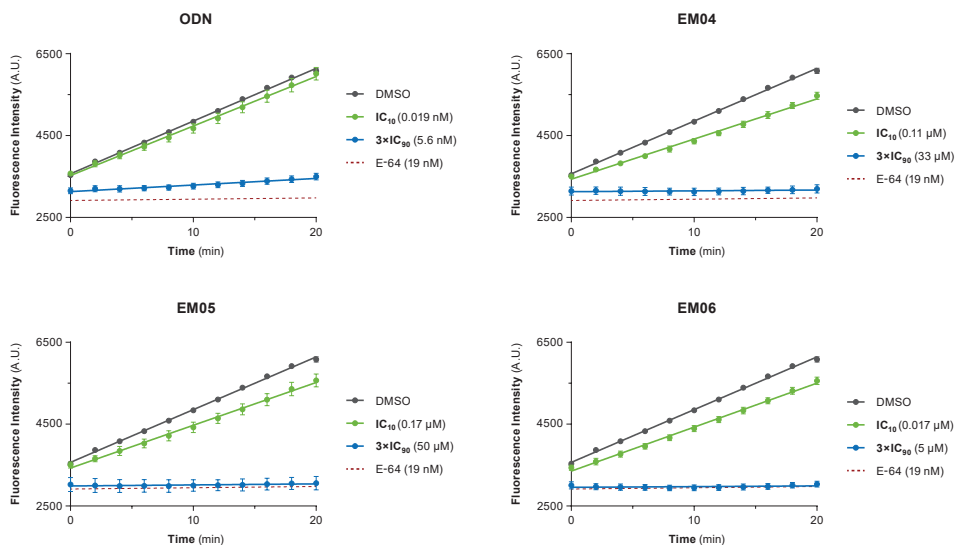
7.4. Jump Dilution Assay

Figure S3 | CatK activity in control samples without dilution (jump dilution assay). Data accompanying **Figure 4**. Recombinant CatK was preincubated with inhibitor followed by addition of substrate Z-FR-AMC (final conc. 4 μM) to establish inhibitory potency without dilution. Inhibitor concentrations shown are after addition of Z-FR-AMC substrate, and correlate with the inhibitor concentration before and after 300-fold dilution in the jump dilution assay (progress curves shown in **Figure 4B**). E-64 is the full inhibition control *(dashed line)*.

7.5. Bottom-up MS Analysis

Sequence mature human **CatK** (Uniprot; P43235), with underlined proteolytic peptide containing catalytic residue (Cys25) after trypsin digestion;

```
GYVTPVKNQG QCGSCWAFSS VGALEGQLKK KTGKLLNLSP QNLVDCVSEN DGCGGGYMTN AFQYVQKNRG IDSEDAYPYV
GQEESCMYNP TGKAAKCRGY REIPEGNEKA LKRAVARVGP VSVAIDASLT SFQFYSKGVY YDESCNSDNL NHAVLAVGYG
IQKGNKHWII KNSWGENWGN KGYILMARNK NNACGIANLA SFPKM
```

Table S2 | Tryptic peptides identified with Mascot (v2.2.04) after alkylation (using iodoacetamide) and tryptic digestion of recombinant hCatK or covalent hCatK–EM04 adduct.

	Unbound hCatK	hCatK–EM04
Peptide sequence	NQGQCGSCWAFSSVGALEGQLKK C5-carbamidomethyl (57.02 Da) C8-carbamidomethyl (57.02 Da)	NQGQCGSCWAFSSVGALEGQLKKK C5-carbamidomethyl (57.02 Da) C8-EM04 (498.16 Da)
Charge	+3	+4
Monoisotopic m/z	838.1 Da	771.11 Da

Bottom-up MS analysis. For the hCatK–EM04 adduct, double carbamidomethylated peptide NQGQC*GSC*WAFSSVGALEGQLKK$_{18-40}$ disappears nearly completely, with appearance of peptide NQGQC*GSC@WAFSSVGALEGQLKKK$_{18-41}$ with a single carbamidomethyl (*) and a single warhead (@).

Table S3 | Tandem MS analysis. Detected fragment ions of modified tryptic CatK–EM04 peptide.

Sequence	y^+	y^{2+}	$y_\#$
N			24
Q			23
G			22
Q			21
C*			20
G			19
S			18
C@			17
W		875.0	16
A		782.0	15
F		746.3	14
S		672.9	13
S		629.4	12
V	1170.7	585.9	11
G	1071.7	536.3	10
A	1014.6		9
L	943.6		8
E	830.5		7
G	701.5		6
Q	644.4		5
L			4
K	403.3		3
K	275.2		2
K			1

Tandem MS analysis for NQGQC*GSC@WAFSSVGALEGQLKKK peptide (m/z = 771.11 [4+]) related to **Table S2**. Obtained by alkylation and trypsin digestion of covalent CatK–EM04 adduct. * = carbamidomethyl. @ = EM04.

7.6. Protein Crystallography

A

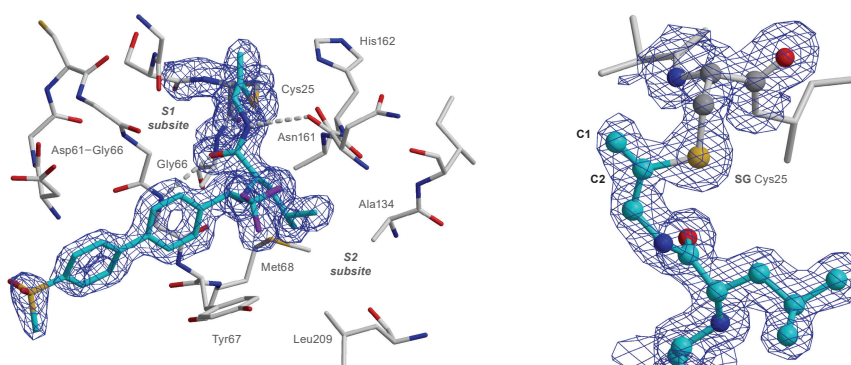| Data Collection		Refinement	
Unit cell		PDB ID	6QBS
a, b, c	75.351, 75.351, 340.184 Å	Resolution range	47.09 – 1.7 Å
α, β, γ	90.0°, 90.0°, 120.0°	No. reflections in working set	64031
Space group	P61 2 2 (number 178)	No. reflections in test set	64031
Molecules per au	2	*R*-kick value	21.0
Wavelength	0.97912 Å	RMSD	
Resolution range	47.09 – 1.7 Å	RMSD Bond lengths	0.02 Å
No. of unique reflections	64186	RMSD Bond angles	2.0°
Completeness (last shell)	99.9% (99.3%)	No. of atoms in au	4018
Multiplicity (last shell)	33.1 (24)	Protein atoms	3298
R_{meas} (last shell)	0.177% (0.978%)	Water molecules	654
I/σ	16.3 (2.2)	Cl$^-$	2
		Ca^{2+}	1
		Mean B value	19.3 Å^2
		Ramachandran plot statistics	
		Favored	412
		Allowed	14
		Outliers	0

4

B

Figure S4 | Protein crystallography of alkyne **EM07** bound covalent to catalytic Cys25 in CatK. Data accompanying **Figure 6**. **(A)** Data collection and refinement statistics for covalent CatK–EM07 adduct. **(B)** Free kick weighted electron density map [42] around inhibitor **EM07** and Cys25. Blue represents maximum-likelihood free-kick (ML FK) map contoured at 1.3 σ. Relevant CatK residues are shown with stick model. Inhibitor is shown in stick model *(left)* or ball-and-stick model *(right)*. Nitrogen, oxygen, fluorine, and sulfur atoms are shown in blue, red, violet, and yellow, respectively. Carbon atoms of **EM07** and CatK are shown in cyan and gray, respectively.

7.7. Kinetic Evaluation

Assay conditions were optimized to obtain a robust signal with a linear increase in product formation for 60 minutes, but a strictly linear rate of product formation for the DMSO control could not be obtained ($k_{ctrl} > 0$). Full curves and fits are shown in **Figure S5**.
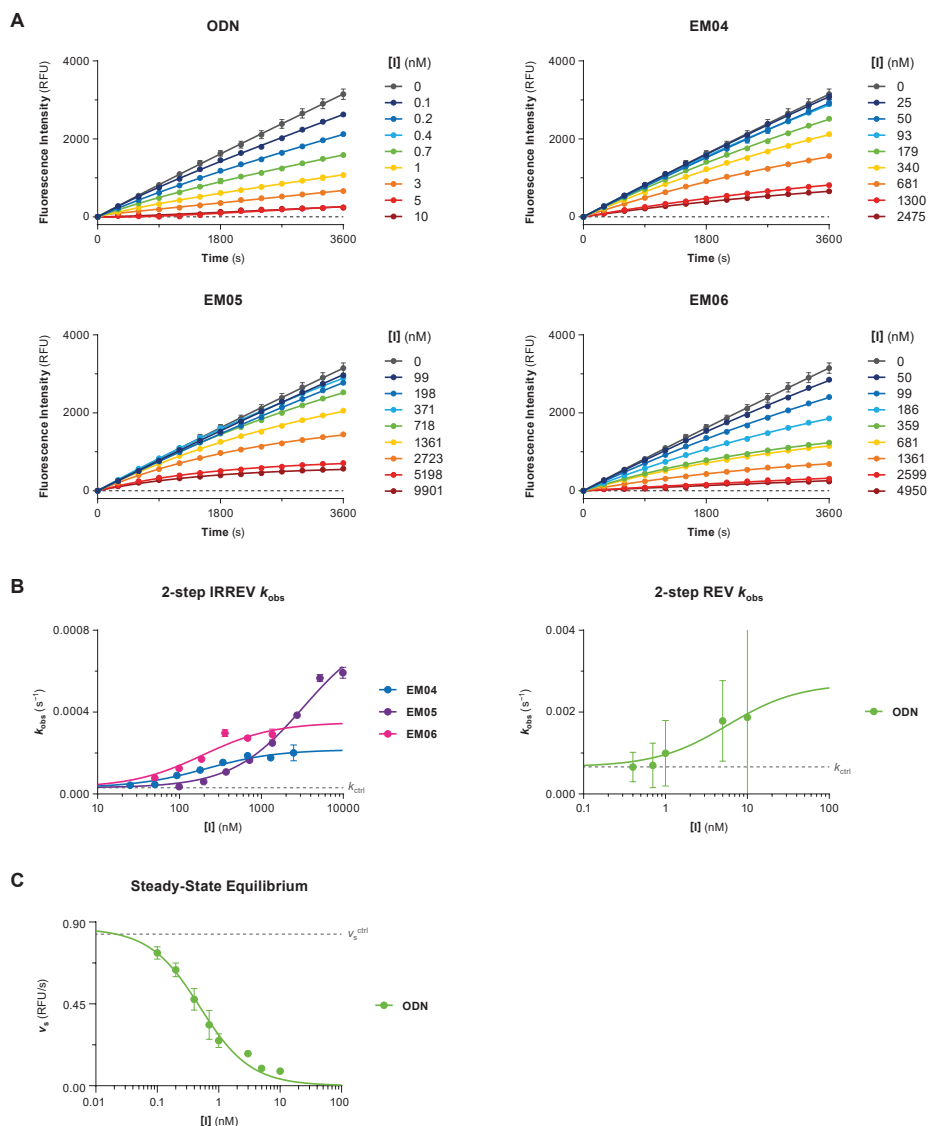

Figure S5 | Kinetic evaluation of covalent inhibitors. Data accompanying **Table 2**. **(A)** Progress curves for baseline-corrected substrate hydrolysis were fitted to one-phase exponential association (constrained v_s = 0 for irreversible inhibitors) to find k_{obs}. **(B)** Plots of k_{obs} against inhibitor concentration were fitted to their respective equations – based on inhibitor binding mode – to obtain relevant kinetic parameters. **(C)** Plot of v_s against inhibitor concentration was fitted to Morrison's quadratic equation to obtain steady-state equilibrium constant K_i^*.

7.8. Human Osteoclast Assays

Bone resorption quantification. The total bone resorption area was quantified because bone resorption by osteoclasts is not homogeneously distributed over bone slices, and it can be hard to select representative areas on the bone (**Figure S6B**). Please note that this only considers the area of resorption, not the depth of the resorption pits: trenches are deeper than pits, so more bone is resorbed in the same area. An overview to compare the total bone resorption on a bone slices, as judged by visual assessment, has also been included (**Figure S6C**). A larger number of resorption areas correlates with more active, resorbing osteoclasts. Trenches are characteristic of fully functional osteoclasts; pits are more commonly seen in osteoclasts with impaired CatK activity. However, trenches and pits can be observed in both cases, possibly because mature osteoclasts are formed between day 3 and day 7 (in absence of inhibitor): osteoclasts that matured before day 7 already started to resorb the bone before inhibitor treatment was started.
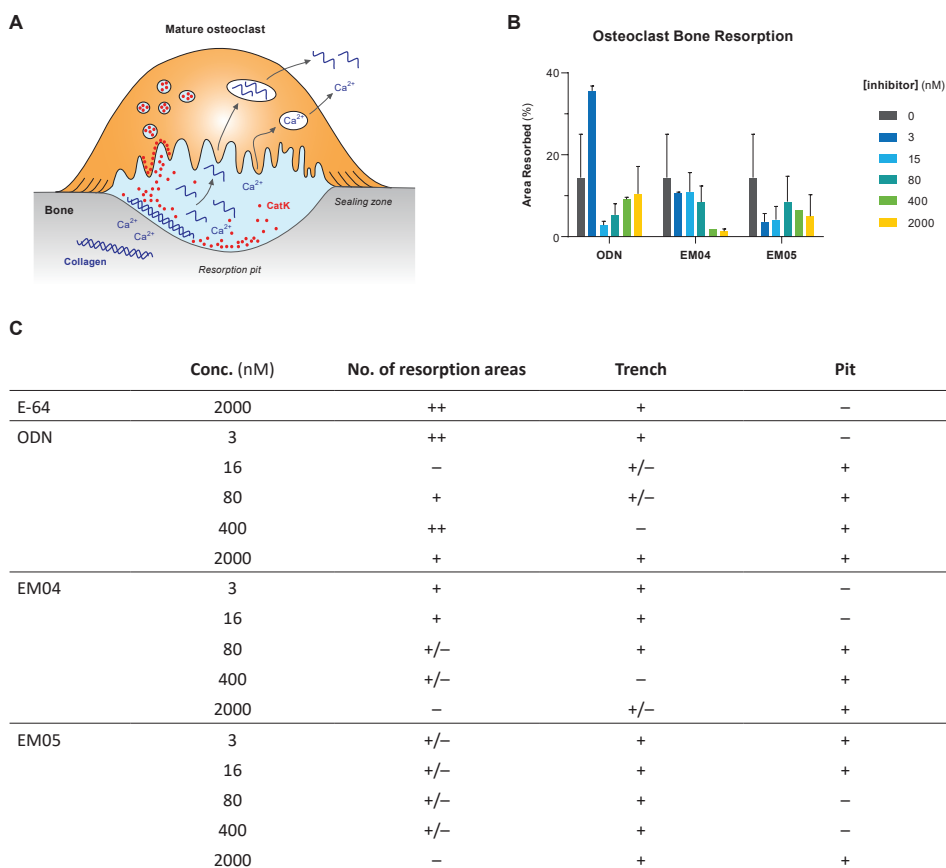
C

	Conc. (nM)	No. of resorption areas	Trench	Pit
E-64	2000	++	+	−
ODN	3	++	+	−
	16	−	+/−	+
	80	+	+/−	+
	400	++	−	+
	2000	+	+	+
EM04	3	+	+	−
	16	+	+	−
	80	+/−	+	+
	400	+/−	−	+
	2000	−	+/−	+
EM05	3	+/−	+	+
	16	+/−	+	+
	80	+/−	+	−
	400	+/−	+	−
	2000	−	+	+

Figure S6 | Bone resorption by human osteoclasts. Data accompanying **Figure 7B**. **(A)** Schematic overview of osteoclast bone resorption. A resorbing osteoclast secretes lysosomal CatK into the acidified resorption lacunae, resulting in degradation of collagen I and bone demineralization. Adapted from Rodan and Duong.[84] **(B)** Quantification of bone resorption area. Bone resorption quantified as percentage of the total area on each bone slice. This measurement does not distinguish between pits and trenches, so depth of the resorption pit is not taken into account. **(C)** Qualitative assessment of bone resorption profile.

TRAcP staining and cell counting. Mature, resorbing osteoclasts are multinucleated and are TRAcP positive. Tartrate-resistant acid phosphatase (TRAcP) is a commonly used histochemical marker of osteoclasts, and secretion of TRAcP is correlated with resorptive behavior.[85] TRAcP is upregulated upon selective CatK inhibition (either genetic or pharmaceutical).[56] The number of mature osteoclasts increased upon treatment with high inhibitor concentrations (**Figure S7**).

qABP labeling. Osteoclast (OC) lysates were incubated with quenched activity-based probe (qABP) BMV109, that forms a fluorescent protease–qABP adduct with active, uninhibited protease (**Figure S8A**, see also **Figure S2**). Fluorescence scan reveals that only small amounts of mature CatK are present in DMSO-treated OCs, possibly because mature CatK is self-degrading. Coomassie protein staining shows that differences in mature CatK are not the result of loading differences. The observed CatK activity in ODN-treated OC lysates is an artifact and does not reflect CatK activity in the lysate: excess of irreversible qABP can outcompete reversible inhibitor ODN from CatK–ODN complexes and adducts.

Western Blotting. Osteoclast lysates were loaded as concentrated as possible (10 µL/lane) because the CatK concentration in OC lysate is otherwise too low for detection, even when using an HRP secondary antibody to amplify the signal. The different CatK species – full-length $proCatK_{1-329}$, $proCatK_{16-329}$ without the signal peptide, and mature $CatK_{115-329}$ – can clearly be identified in the mature CatK and proCatK controls (**Figure S8B-C**). An increase in mature CatK is observed for ODN (all concentrations), and high concentrations of EM04 and EM05.
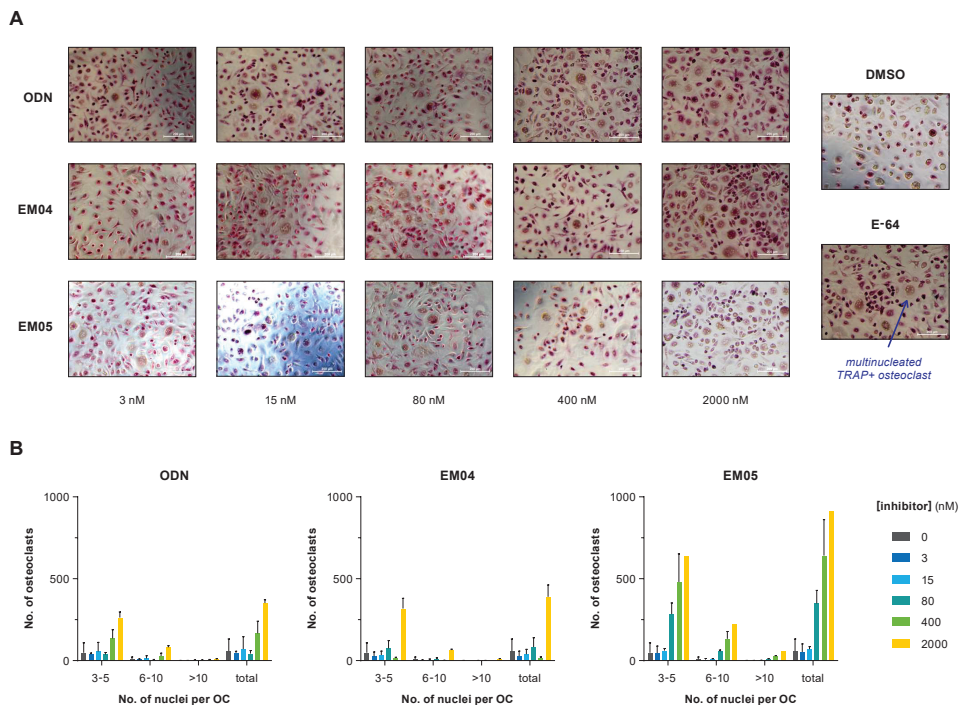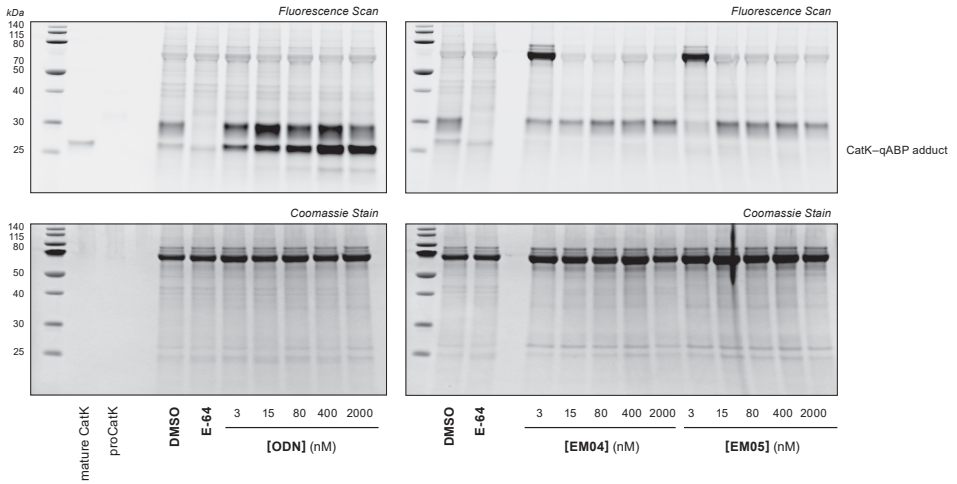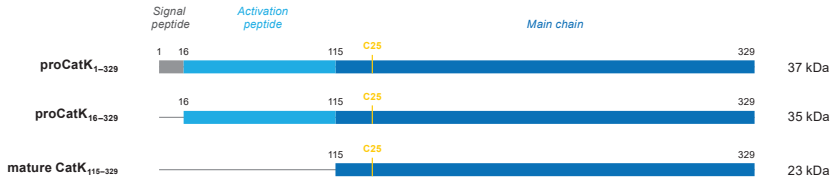

Figure S7 | Counting mature OCs on plastic. **(A)** Representative TRAcP-stained OCs on plastic treated with ODN, EM04 or EM05. **(B)** Osteoclast formation on plastic with different inhibitor concentrations. For all inhibitors, an increase in the number of mature OCs is observed at high inhibitor concentration.

A   **CatK activity in OCs**

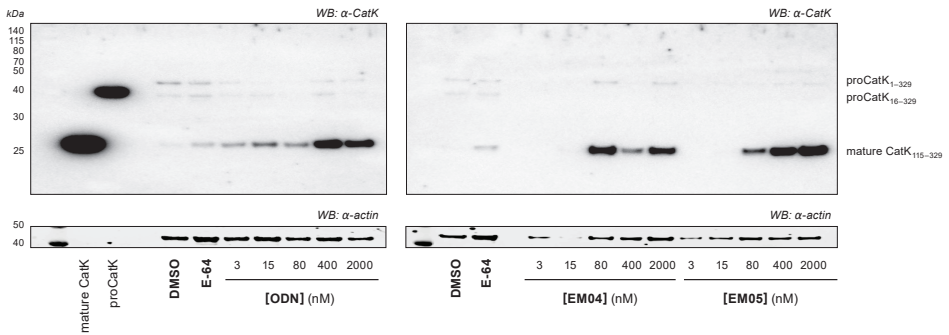
B

4

C   **CatK expression in OCs**

Figure S8 | CatK activity and expression in osteoclast (OC) lysates. Data accompanying **Figure 7C**. **(A)** Full gel scans for OC lysates treated with qABP BMV109 (1 μM) for 2 h. Darker bands = more CatK activity. *Top:* Fluorescence scan (λ_{ex} = 635 nm, λ_{em} = 665 nm) for protease–qABP adducts. *Bottom:* Coomassie protein stain as loading control. **(B)** Schematic overview of various cathepsin K species. Inactive proCatK is activated by acid-mediated autoproteolysis to form mature, active CatK.[55] **(C)** Full blots for OC lysates. *Top:* anti-CatK (chemiluminescence). *Bottom:* anti-Actin (λ = 785 nm).